Supplementary Information

Arylation of Gold Nanoclusters and Insights in Structure-Related CO_2 Reduction Reaction Performances

Chen Zhu,[†,‡] Bo Li,[§,‡] Chen Li[†], Luyao Lu,[†] Hao Li,[†] Xinhua Yuan,[†] Xi Kang,[†,*] De-en Jiang,[§,*] Manzhou Zhu[†,*]

†Department of Chemistry and Centre for Atomic Engineering of Advanced Materials, Anhui Province Key Laboratory of Chemistry for Inorganic/Organic Hybrid Functionalized Materials, Key Laboratory of Structure and Functional Regulation of Hybrid Materials, Anhui University, Ministry of Education, Anhui University, Hefei, Anhui 230601, P. R. China.

§Department of Chemical and Biomolecular Engineering, Vanderbilt University, Nashville, Tennessee 37235, United States.

*E-mails of corresponding authors: kangxi_chem@ahu.edu.cn (X.K.); de-en.jiang@vanderbilt.edu (D.-e. J.); zmz@ahu.edu.cn (M.Z.)

Notes: The authors declare no competing financial interest.

This Supplementary Information file includes:

Experimental Methods

Materials

All following reagents were purchased from Sigma-Aldrich and used without further purification: tetrachloroauric(III) acid ($HAuCl_4 \cdot 4H_2O$, 99% metal basis), bis(2-diphenylphosphinophenyl)ether (DPPOE, 98%), *p*-toluenethiol (97%), sodium tetraphenylborate ($NaBPh_4$), sodium tetrakis(4-fluorophenyl)borate ($NaB(Ph\text{-}F)_4$), potassium tetrakis(4-chlorophenyl)borate ($KB(Ph\text{-}Cl)_4$), sodiumborohydride ($NaBH_4$, 99%), methylene chloride (CH_2Cl_2, HPLC grade), methanol (CH_3OH, HPLC grade), n-Hexane (C_6H_{14}, HPLC grade).

Synthesis of the $[Au_{15}(DPPOE)_3(S\text{-}Ph^pMe)_6]^+$ nanocluster (Au_{15}-SR)

80 mg of $HAuCl_4 \cdot 4H_2O$ were dissolved in a mixed solution (15 mL of CH_2Cl_2 and 5 mL of CH_3OH). The solution was vigorously stirred with a magnetic stir bar for 5 minutes, and 50 mg of *p*-toluenethiol was added. After 20 minutes, 50 mg of DPPOE was added, and the reaction was further stirred for 20 minutes. Then, 5 mL of an aqueous solution of $NaBH_4$ (8 mg mL^{-1}) was added, and the solution color changed to black immediately. The reaction was proceeded for 24 hours. After evaporating all solvent, the crude product was dissolved in 5 mL of CH_2Cl_2 and centrifuged at 10000 rpm for 1 minute to remove the precipitate. Then, the crude product was washed with Hex three times (20 mL × 3) to get the cluster product and purified by thin layer chromatography (TLC). Finally, the precipitate was dissolved in CH_2Cl_2, which produced the Au_{15}-SR nanocluster. The synthetic yield was calculated to be 9% based on the Au element for the Au_{15}-SR nanocluster.

Synthesis of $[Au_{15}(DPPOE)_3(S\text{-}Ph^pMe)_4(Ph)_2]^+$ nanocluster (Au_{15}-Ph)

10 mg of the Au_{15}-SR nanocluster was dissolved in 10 mL DCM, then 10 mg of $NaBPh_4$ dissolved in 5 ml MeOH was added. The solution was quickly stirred with a magnetic stirrer for 5 minutes. Then, the precipitate was collected and washed three times with CH_3OH (20 mL × 3) to remove the redundant $NaBPh_4$ and the by-products (e.g., BPh_3 and thiolates). Finally, the precipitate was dissolved in CH_2Cl_2 and diffused with DCM:Hex=1:3 liquid phase. After 7 days, Au_{15}-Ph nanoclusters crystal was formed. The synthetic yield was calculated to be 58% based on the Au_{15}-SR nanocluster.

Synthesis of $[Au_{15}(DPPOE)_3(S\text{-}Ph^pMe)_4(Ph\text{-}F)_2]^+$ nanocluster (Au_{15}-Ph-F)

The synthesis of Au_{15}-Ph-F was the same as the synthetic procedure of Au_{15}-Ph, just by altering the $NaBPh_4$ precursor to the $NaB(Ph\text{-}F)_4$. The synthetic yield was calculated to be 53% based on the Au_{15}-SR nanocluster.

Synthesis of $[Au_{15}(DPPOE)_3(S\text{-}Ph^pMe)_4(Ph\text{-}Cl)_2]^+$ nanocluster (Au_{15}-Ph-Cl)

The synthesis of Au_{15}-Ph-F was the same as the synthetic procedure of Au_{15}-Ph, just by altering the $NaBPh_4$ precursor to the $KB(Ph\text{-}Cl)_4$. The synthetic yield was calculated to be 48% based on the Au_{15}-SR nanocluster.

Characterizations

The optical absorption (UV-vis) spectra of nanoclusters were recorded using an Agilent 8453 diode array spectrometer.

The electrospray ionization-mass spectrometry (ESI-MS) measurements were performed by

Waters XEVO G2-XS QT of the mass spectrometer. The sample was directly infused into the chamber at 5 μL/min. For preparing the ESI samples, nanoclusters were dissolved in CH_2Cl_2 (1 mg/mL) and diluted (v/v = 1:1) by CH_3OH.

The X-ray photoelectron spectroscopy (XPS) measurements were performed on a Thermo ESCALAB 250 instrument configured with a monochromatized Al Kα (1486.8 eV) 150 W X-ray source, 0.5 mm circular spot size.

The thermogravimetric analysis (TGA) was carried out on a thermogravimetric analyzer (DTG-60H, Shimadzu Instruments, Inc.) with 5 mg of nanoclusters in a SiO_2 pan heating rate of 10°C min^{-1} (nitrogen atmosphere) from room temperature to 800°C.

Nuclear Magnetic Resonance (NMR) measurements were carried out on JEOL JNM ECZ400R at 300K.

X-Ray Crystallography

The data collection for single-crystal X-ray diffraction (SC-XRD) of all nanocluster crystal samples was carried out on Stoe Stadivari diffractometer under nitrogen flow, using graphite-monochromatized Cu Kα radiation (λ = 1.54186 Å). Data reductions and absorption corrections were performed using the SAINT and SADABS programs, respectively. The structure was solved by direct methods and refined with full-matrix least squares on F^2 using the SHELXTL software package. All non-hydrogen atoms were refined anisotropically, and all the hydrogen atoms were set in geometrically calculated positions and refined isotropically using a riding model. All crystal structures were treated with PLATON SQUEEZE. The diffuse electron densities from these residual solvent molecules were removed. The CCDC number of the Au_{15}-Ph nanocluster was 2307548. The CCDC number of the Au_{15}-Ph-F nanocluster was 2307549. The CCDC number of the Au_{15}-Ph-Cl nanocluster was 2307550.

Electrochemical measurements. All electrochemical tests are conducted in an H-type electrolysis cell, with two compartments separated by a Nafion 117 proton exchange membrane. Carbon paper loaded with ink reagent was used for CO_2 reduction of the working electrode. Additionally, an Ag/AgCl electrode serves as the reference electrode, while a platinum electrode functions as the auxiliary electrode. Au_{15}-Ph and Au_{15}-SR nanoclusters were loaded on activated carbon with a mass ratio of 1:10. After the sample was dried, the catalytic sample was dispersed in a mixture of ethanol, water and Nafion (10mg/mL) for 30 min by ultrasonic treatment to prepare ink reagent. The working electrode is then prepared by applying 200 μL ink droplets onto the carbon paper. The electrolyte is 0.5 M $KHCO_3$ solution. The reactants were quantified using a PANNA A91 PLUS gas phase detector with an FID detector. The whole CO_2RR reacts for 10 min, and during the reaction, the electrolyte in the cathode chamber is stirred at a speed of 600rpm. The uncompensated resistance at each potential is determined using electrochemical impedance spectroscopy (EIS) prior to electrochemical testing and 90%iR correction is performed.

The turnover frequency was calculated as below:

$$TOF = \frac{Iproduct * t}{NFnAu}$$

where, Iproduct = partial current density for certain product (e.g., CO), F = Faradaic constant (96485 C mol^{-1}), N = electron number transferred in CO_2RR, t = reaction time (s), and nAu = mol of active Au sites in CO_2RR (15 Au sites per cluster).

Computational Details. Density functional theory (DFT) calculations were performed with the Gaussian 16 program package[1] using the PBE functional.[2] 6-31G** basis sets[3] were employed for C, H, O, S, P, while LANL2DZ basis set for Au was used.[4] Grimme's D3 with the Becke-Johnson damping method was used to include the dispersion interaction.[5] The IEF-PCM solvation model[6] was employed to calculate the reaction energy in aqueous solution.

The CO_2RR calculations were performed using the Vienna ab initio simulation package (VASP) with the Generalized Gradient Approximation (GGA) of Perdew, Burke, and Ernzerhof (PBE) to describe electron exchange-correlation interactions. A cutoff energy of 400 eV for the plane-wave basis was employed and van der Waals interactions were included using the Grimme's D3 method. Convergence criteria for energy and force are set at 10^{-5} eV and 0.02 eV·A^{-1}, respectively. The Brillouin zone was sampled using Γ point only. The Au_{15}-SR and Au_{15}-Ph complexes were placed in the cubic box of 25×25×25 $Å^3$ and a uniform background charge was added to unit cell to balance the charges.

The reaction free energies of the CO_2RR steps were calculated using the computational hydrogen electrode proposed by Norskov et al. Gibbs free energy (ΔG) for all the reaction steps were computed using the following equation:

$$\Delta G = \Delta E + \Delta E_{ZPE} - T\Delta S,$$

Where ΔE is the difference of the DFT total energy, ΔE_{ZPE} is the zero-point energy difference calculated from the vibrational frequencies, and ΔS the entropy difference between the product and the reactant. The entropies of the free molecules at 298 K and 1 atom were taken from the NIST database, while the vibrational entropy was computed for the adsorbed species.

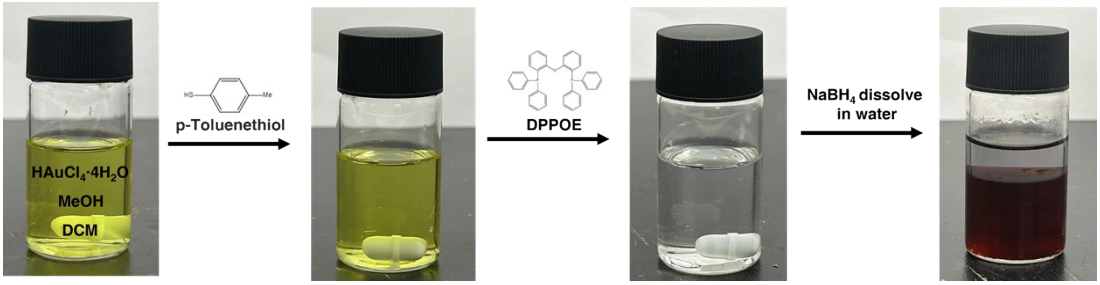

Figure S1. Synthetic approach for the preparation of the Au_{15}-SR nanocluster.

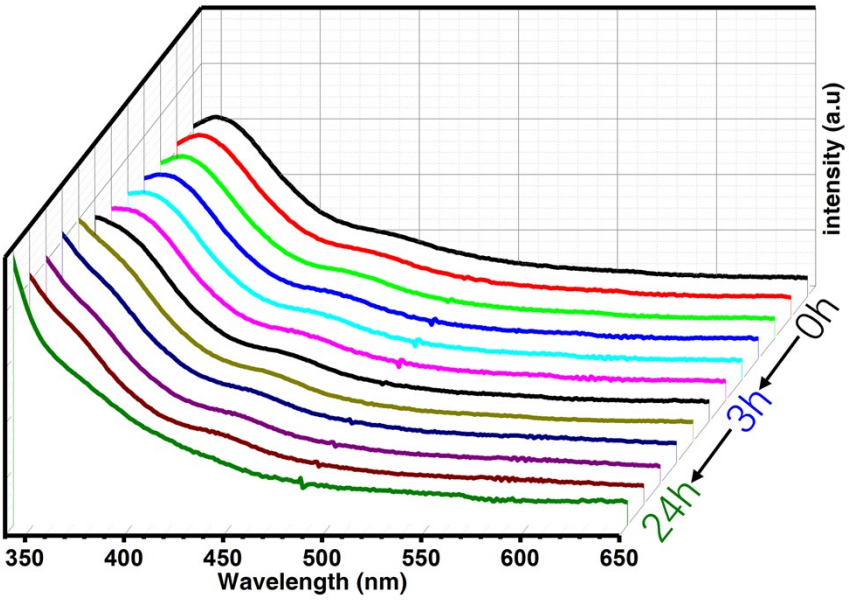

Figure S2. Time-dependent optical absorptions of the Au_{15}-SR nanocluster at room temperature to test the thermal stability of the nanocluster. Characteristic UV-vis absorptions of Au_{15}-SR gradually decreased in intensity after three hours and completely disappeared in approximately 24 hours, indicating degradation.

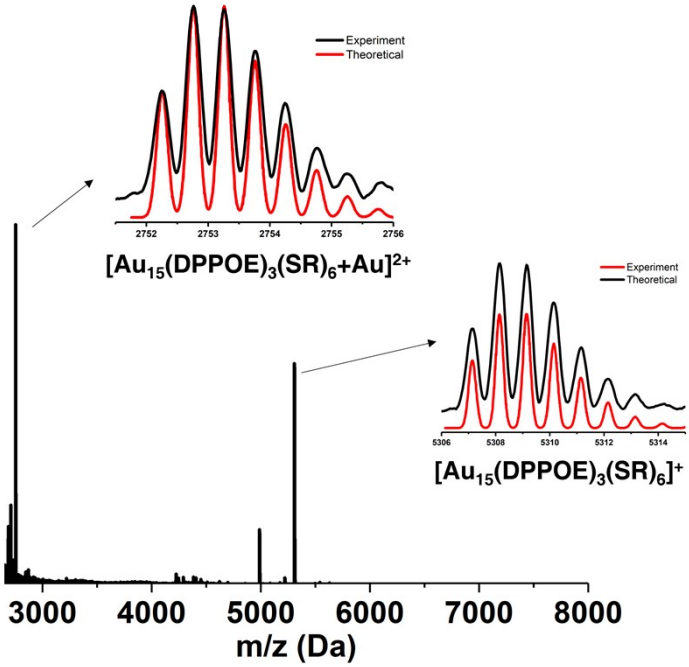

Figure S3. ESI-MS result of the Au_{15}-SR nanocluster. Two mass signals were detected, corresponding to the chemical formula of $[Au_{15}(DPPOE)_3(S\text{-}Ph^pMe)_6]^+$ and $[Au_{15}(DPPOE)_3(S\text{-}Ph^pMe)_6\text{-}Au]^{2+}$. For $[Au_{15}(DPPOE)_3(S\text{-}Ph^pMe)_6\text{-}Au]^{2+}$, a gold cation was anchored onto the cluster framework to promote the cluster ionization.

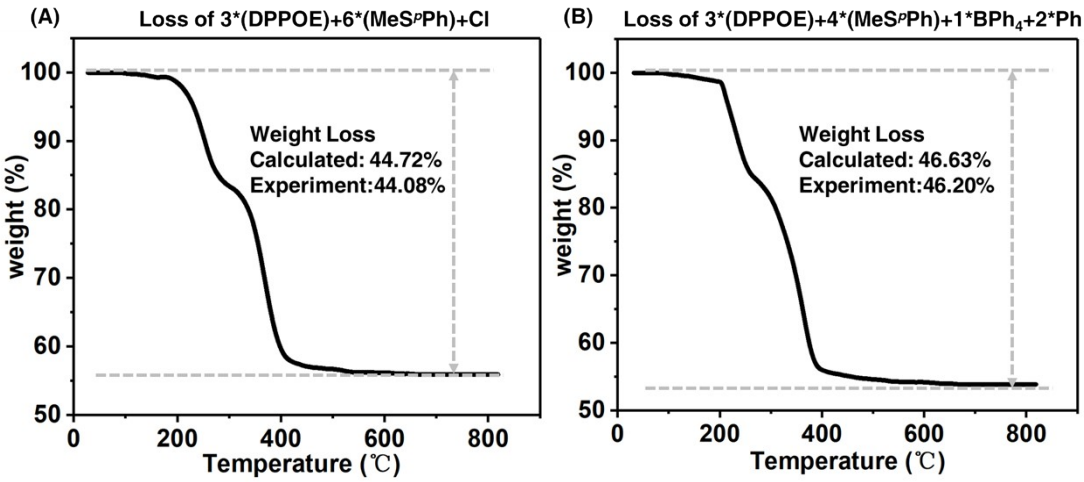

Figure S4. TGA results of (A) the Au_{15}-SR nanocluster and (B) the Au_{15}-Ph nanocluster. The experimental losses matched well with the calculated ones, demonstrating the high purity of the prepared nanoclusters.

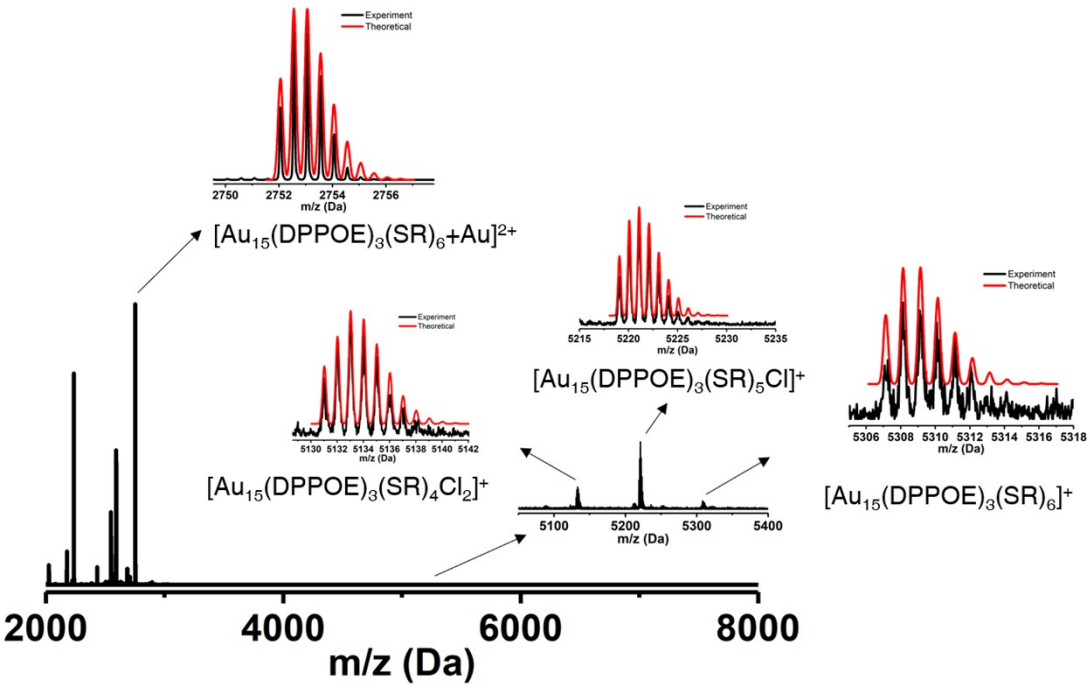

Figure S5. ESI-MS result of the Au_{15}-SR nanocluster in the presence of Cs^+. Four mass signals were detected, corresponding to the chemical formula of $[Au_{15}(DPPOE)_3(S\text{-}Ph^pMe)_6\text{-}Au]^{2+}$, $[Au_{15}(DPPOE)_3(S\text{-}Ph^pMe)_6]^+$, $[Au_{15}(DPPOE)_3(S\text{-}Ph^pMe)_5Cl_1]^+$, and $[Au_{15}(DPPOE)_3(S\text{-}Ph^pMe)_4Cl_2]^+$. In this context, a maximum of two Cl ligands could be arranged onto the cluster surface by substituting the detachable thiol ligands.

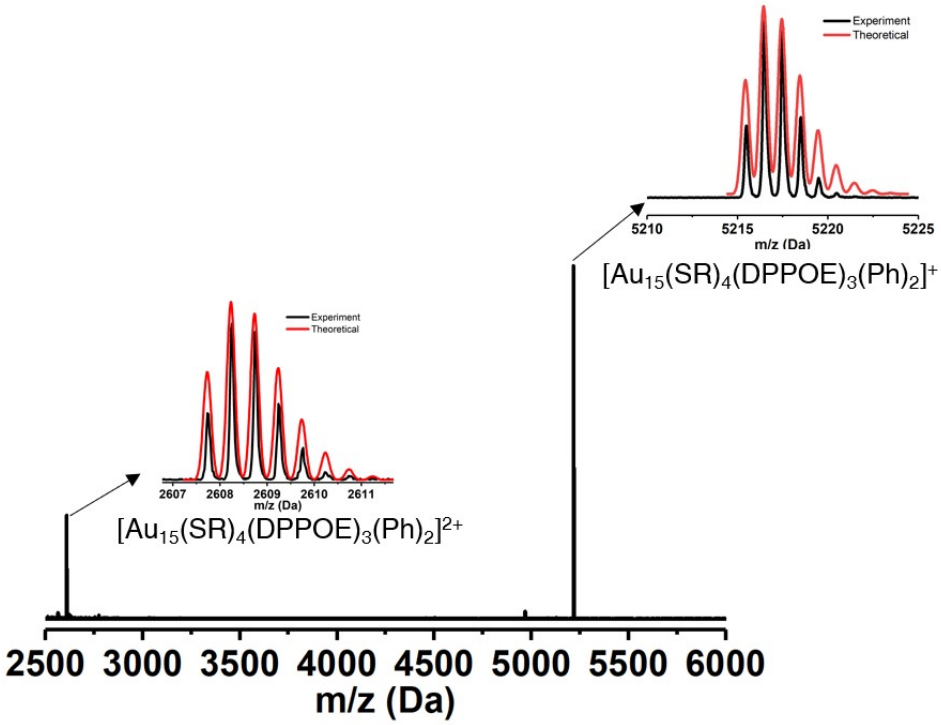

Figure S6. ESI-MS result of the Au_{15}-Ph nanocluster. The cluster sample was prepared by dissolving the cluster crystal with CH_2Cl_2.

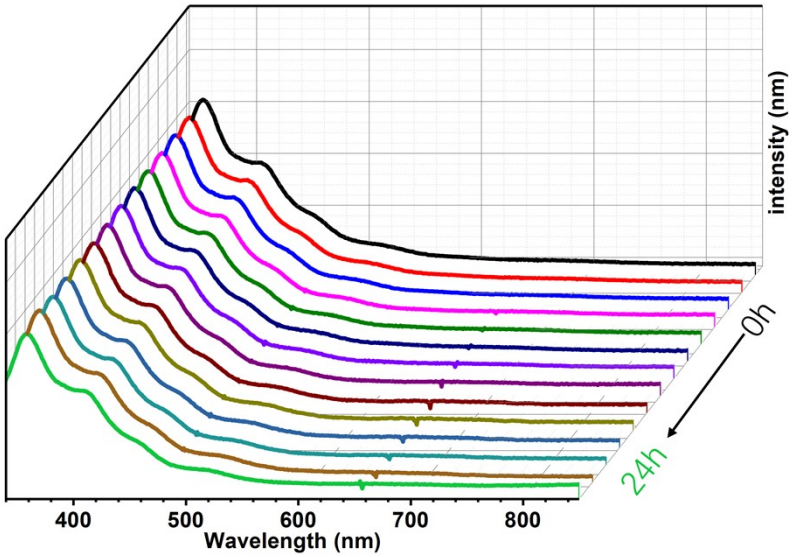

Figure S7. Time-dependent optical absorptions of the Au_{15}-Ph nanocluster at room temperature to test the thermal stability of the nanocluster. Characteristic UV-vis absorptions of Au_{15}-Ph maintained within 24 hours, demonstrating its high stability.

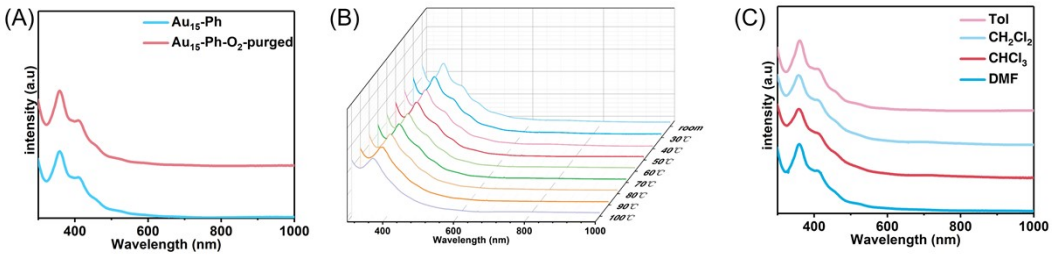

Figure S8. Stability test of Au_{15}-Ph in oxygen, at different temperatures, and in different solvents.

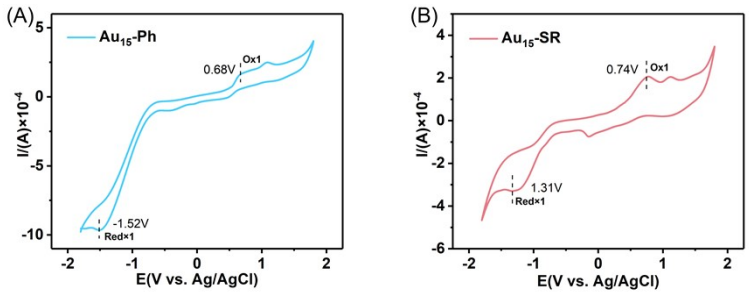

Figure S9. Cyclic Voltammetry (CV) test of Au_{15}-Ph and Au_{15}-SR nanoclusters.

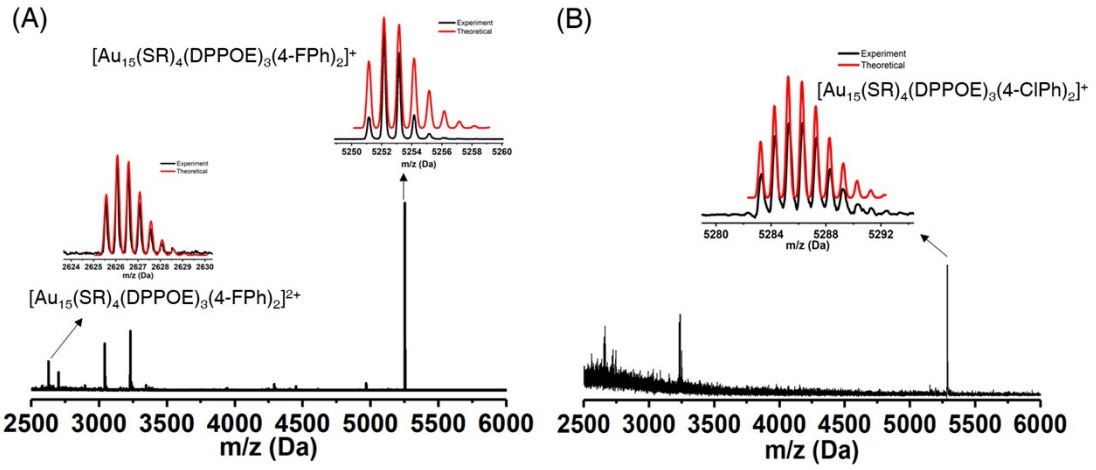

Figure S10. ESI-MS results of (A) the Au_{15}-Ph-F nanocluster and (B) the Au_{15}-Ph-Cl nanocluster. The mass signals of $[Au_{15}(DPPOE)_3(S\text{-}Ph^{p}Me)_4(Ph\text{-}F)_2]^+$ and $[Au_{15}(DPPOE)_3(S\text{-}Ph^{p}Me)_4(Ph\text{-}Cl)_2]^+$ were detected.

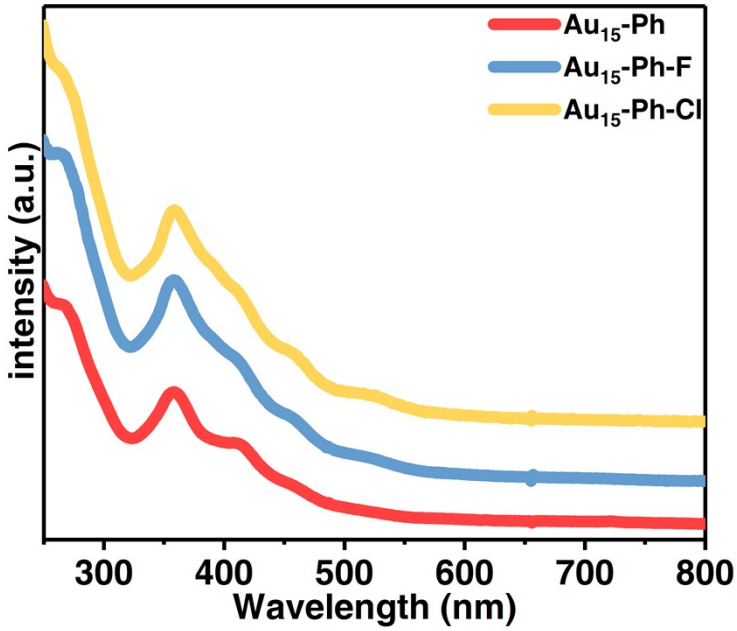

Figure S11. The comparison of optical absorptions of Au_{15}-Ph, Au_{15}-Ph-F, and Au_{15}-Ph-Cl nanoclusters. The optical absorptions of the three nanoclusters were almost the same, demonstrating their analogous electronic structures.

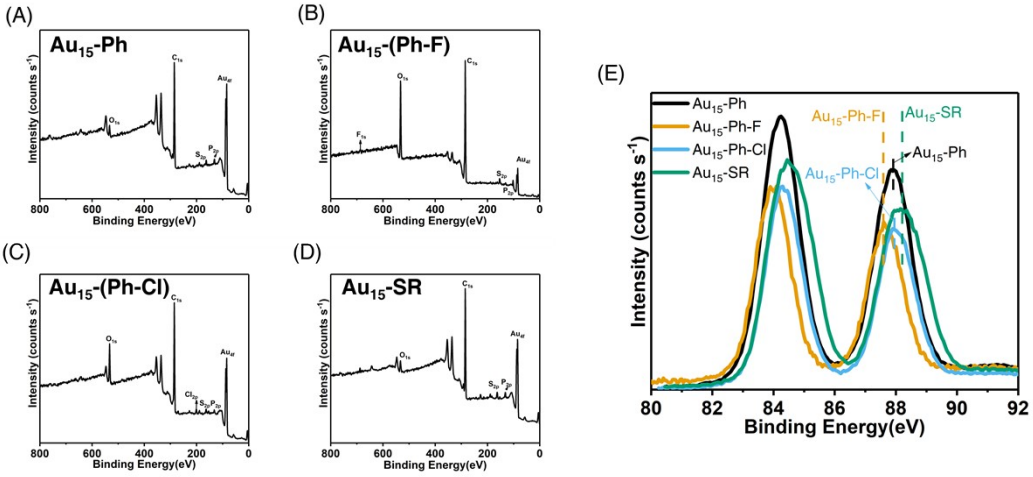

Figure S12. XPS results of Au_{15}-Ph, Au_{15}-Ph-F, Au_{15}-Ph-Cl, and Au_{15}-SR nanoclusters. The bonding energies of Au_{4f} in the three arylgold nanoclusters showed remarkable blue-shifts relative to Au_{15}-SR.

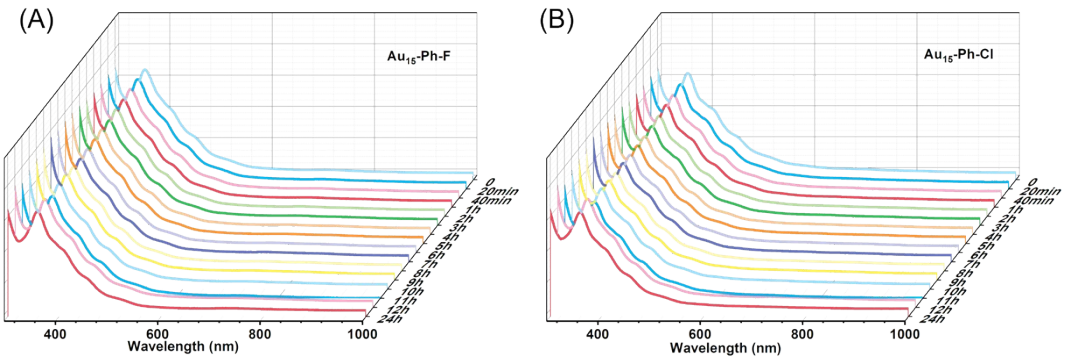

Figure S13. The stability of Au_{15} nanoclusters bearing different aryl groups in 24h.

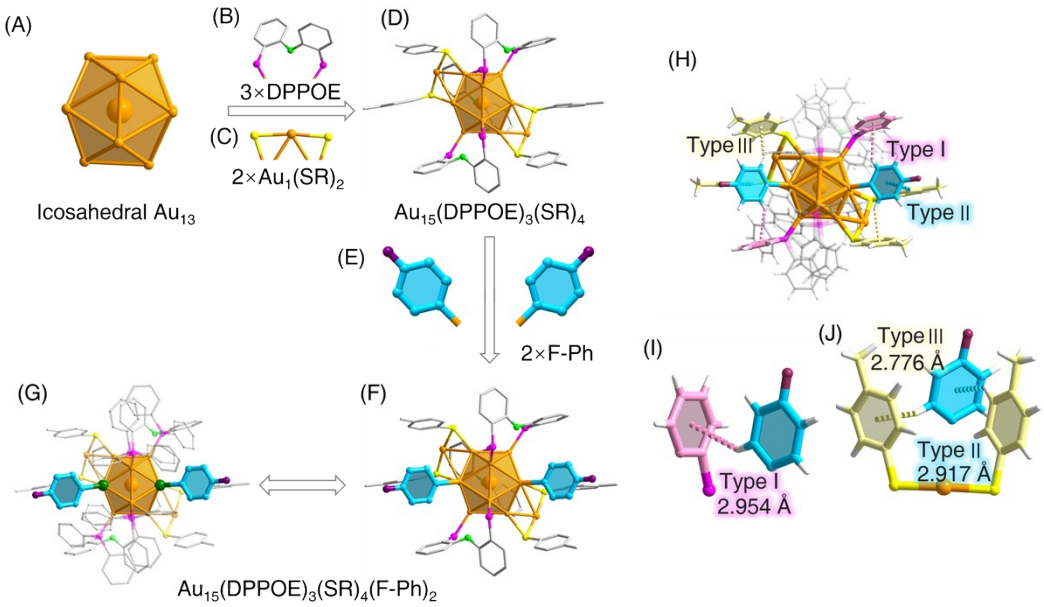

Figure S14. Structural anatomy of the arylgold Au_{15}-Ph-F nanocluster and the intracluster C–H···π interactions to stabilize the aryl ligands on the nanocluster surface.

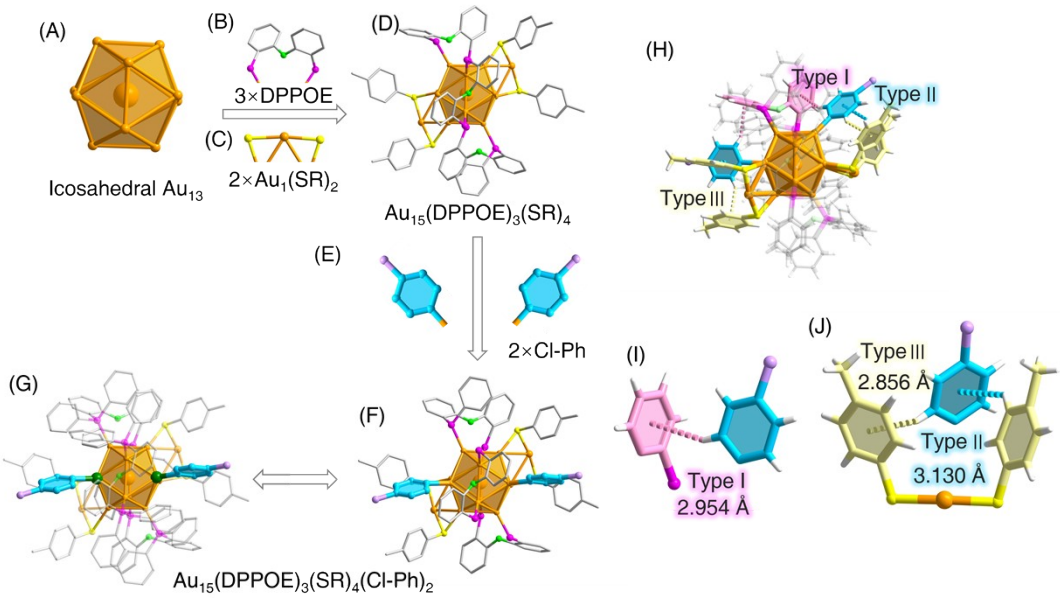

Figure S15. Structural anatomy of the arylgold Au_{15}-Ph-Cl nanocluster and the intracluster C–H···π interactions to stabilize the aryl ligands on the nanocluster surface.

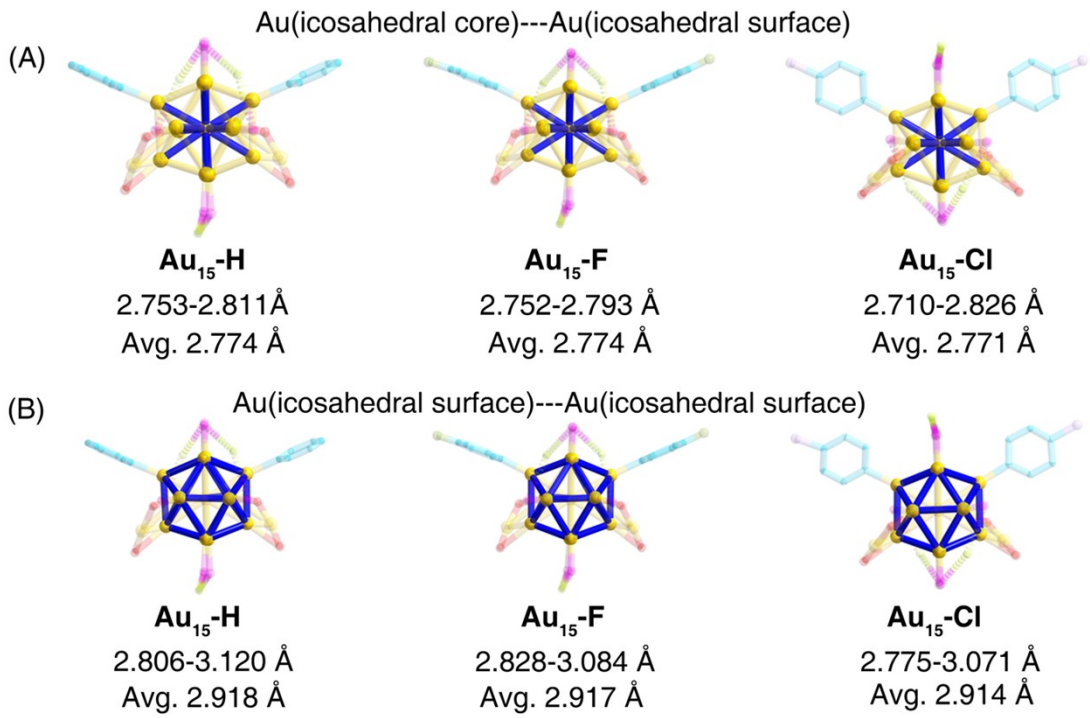

Figure S16. Comparison of the lengths of (A) Au(icosahedral core)-Au(icosahedral core) and (B) Au(icosahedral core)-Au(icosahedral surface) bonds of Au_{15}-Ph, Au_{15}-Ph-F, and Au_{15}-Ph-Cl nanoclusters.

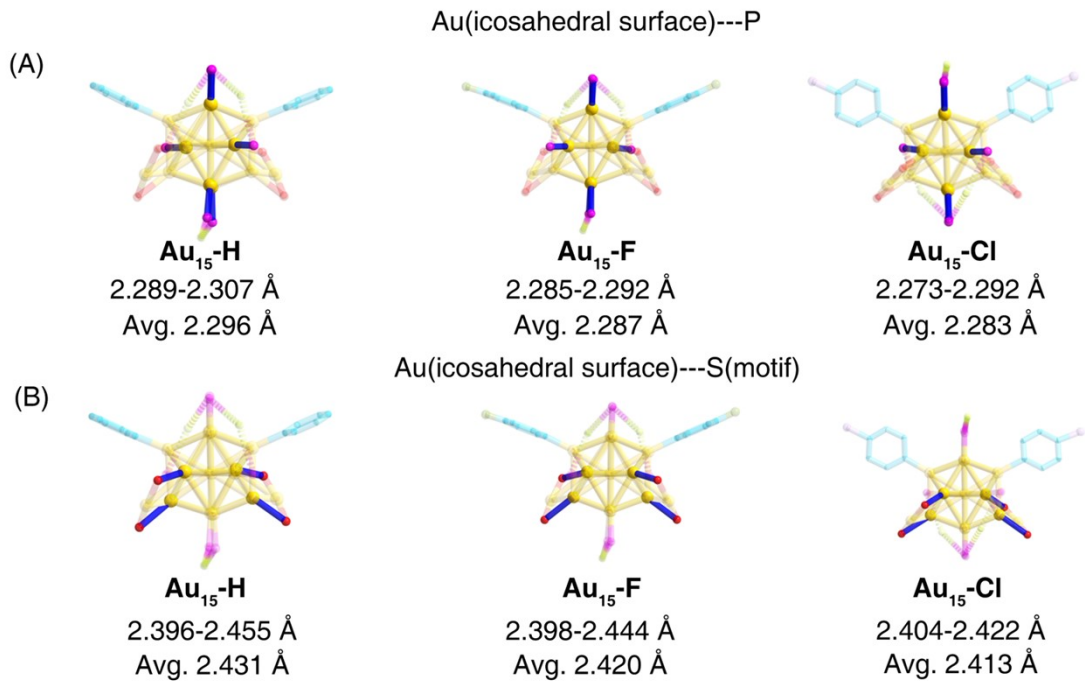

Figure S17. Comparison of the lengths of (A) Au(icosahedral surface)-S(thiol ligand) and (B) Au(icosahedral surface)-P(phosphine ligand) bonds of Au_{15}-Ph, Au_{15}-Ph-F, and Au_{15}-Ph-Cl nanoclusters.

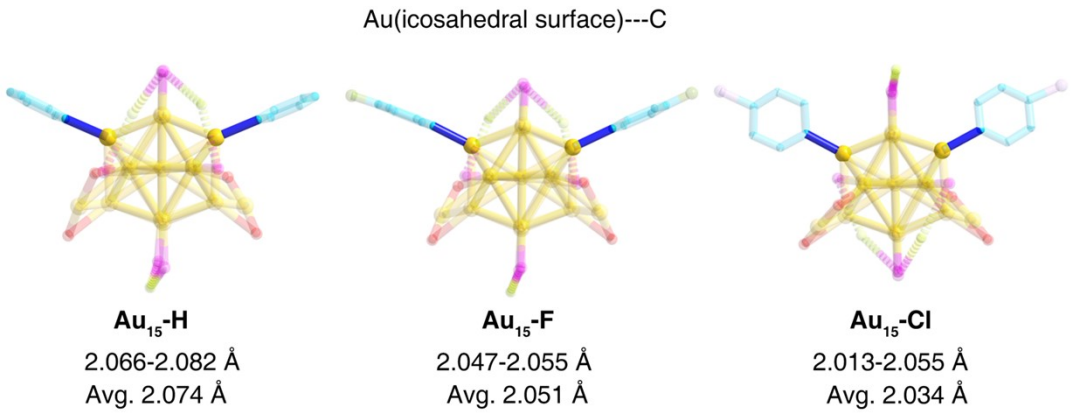

Figure S18. Comparison of the lengths of Au(icosahedral surface)-C(aryl ligand) bonds of Au_{15}-Ph, Au_{15}-Ph-F, and Au_{15}-Ph-Cl nanoclusters.

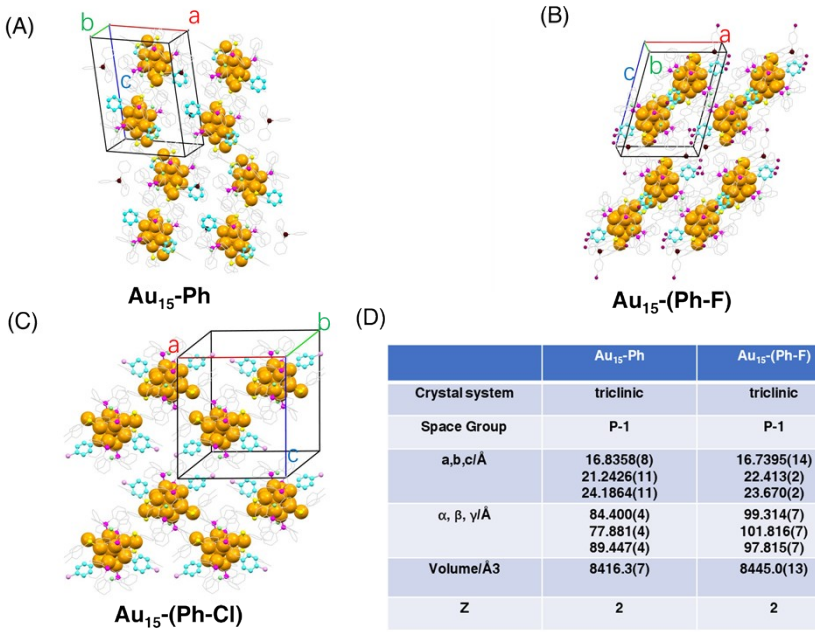

(D)

	Au_{15}-Ph	Au_{15}-(Ph-F)	Au_{15}-(Ph-Cl)
Crystal system	triclinic	triclinic	triclinic
Space Group	P-1	P-1	P-1
a,b,c/Å	16.8358(8) 21.2426(11) 24.1864(11)	16.7395(14) 22.413(2) 23.670(2)	20.4720(11) 21.4293(13) 22.5130(12)
α, β, γ/Å	84.400(4) 77.881(4) 89.447(4)	99.314(7) 101.816(7) 97.815(7)	115.818(4) 93.462(4) 90.360(5)
Volume/Å3	8416.3(7)	8445.0(13)	8868.6(9)
Z	2	2	2

Figure S19. Crystal lattices of (A) Au_{15}-Ph, (B) Au_{15}-Ph-F, and (C) Au_{15}-Ph-Cl nanoclusters. (D) Comparison of the crystalline unit cell parameters of Au_{15}-Ph, Au_{15}-Ph-F, and Au_{15}-Ph-Cl nanoclusters.

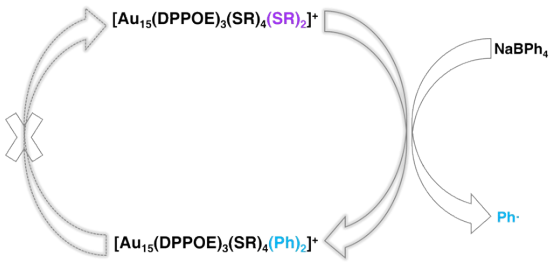

Figure S20. The proposed transforming mechanism of the nanocluster arylation, including the nanocluster arylation from Au_{15}-SR to Au_{15}-Ph and the C-B bond cleavage of $[BPh_4]^-$, referred to the reaction between metal complexes and borate species reported previously.

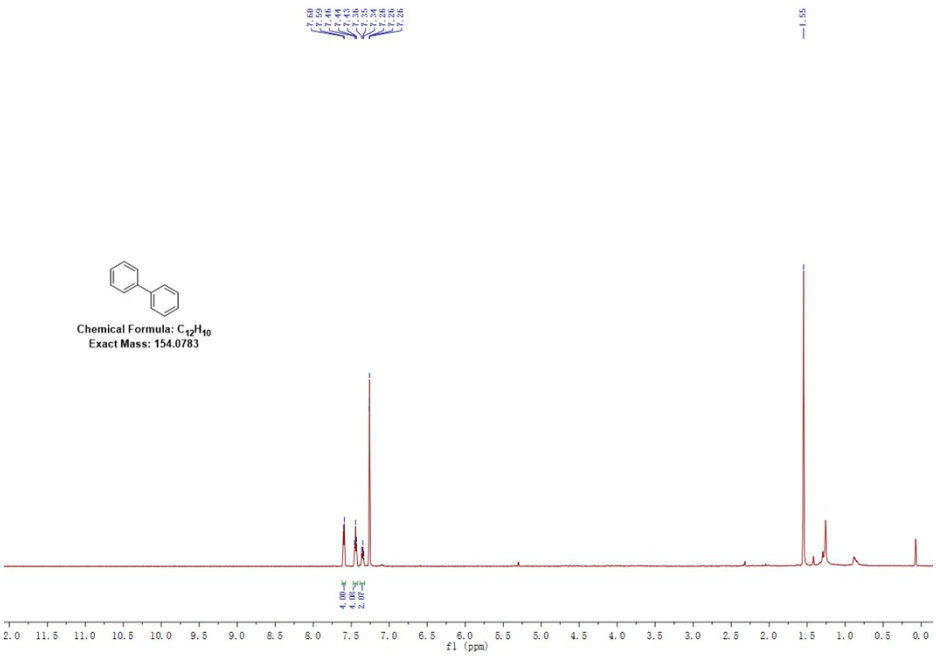

Figure S21. ^{1}H NMR spectrum of diphenyl that was separated from by-products of the nanocluster arylation from Au_{15}-SR to Au_{15}-Ph.

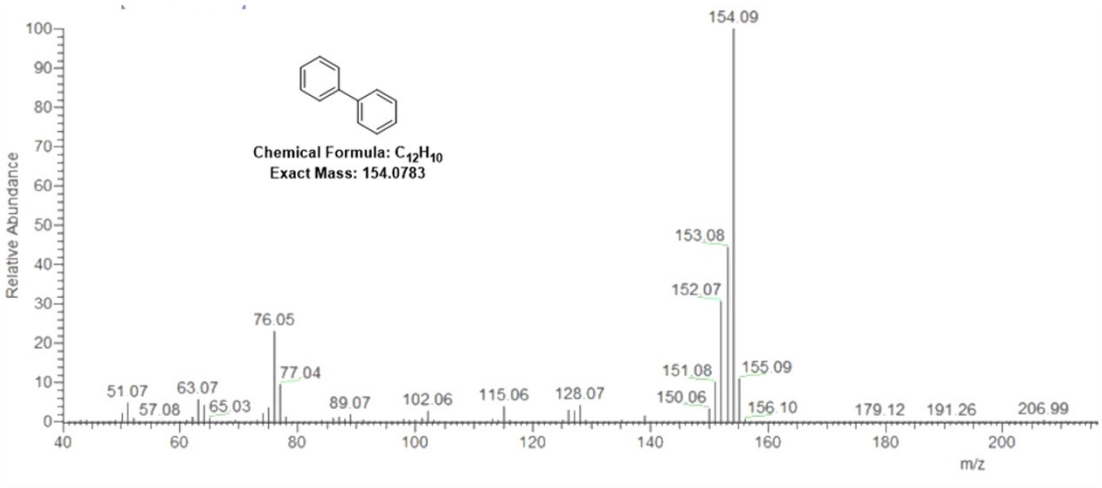

Figure S22. GC-MS result of diphenyl that was separated from by-products of the nanocluster arylation from Au_{15}-SR to Au_{15}-Ph.

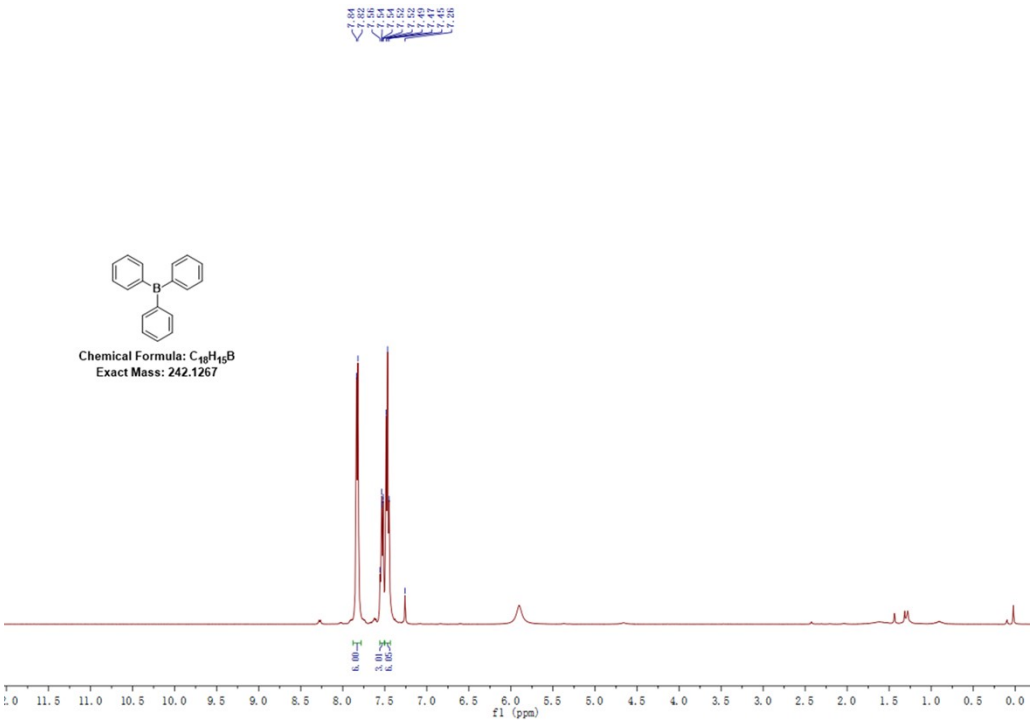

Figure S23. ^{1}H NMR spectrum of BPh_3 that was separated from by-products of the nanocluster arylation from Au_{15}-SR to Au_{15}-Ph.

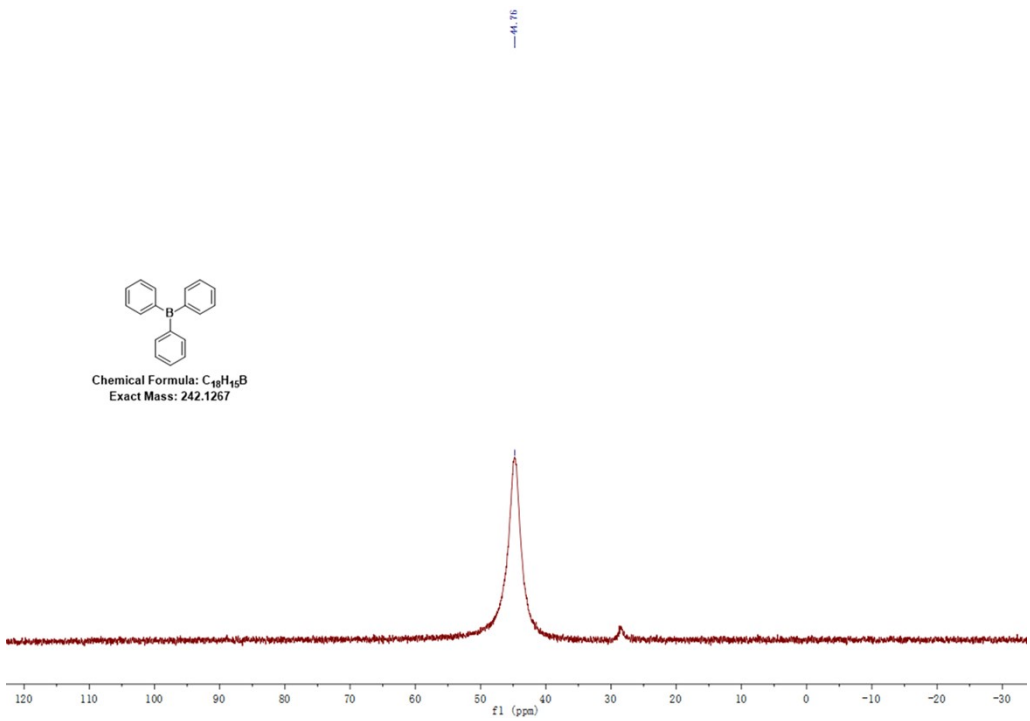

Figure S24. ^{11}B NMR spectrum of BPh_3 that was separated from by-products of the nanocluster arylation from Au_{15}-SR to Au_{15}-Ph.

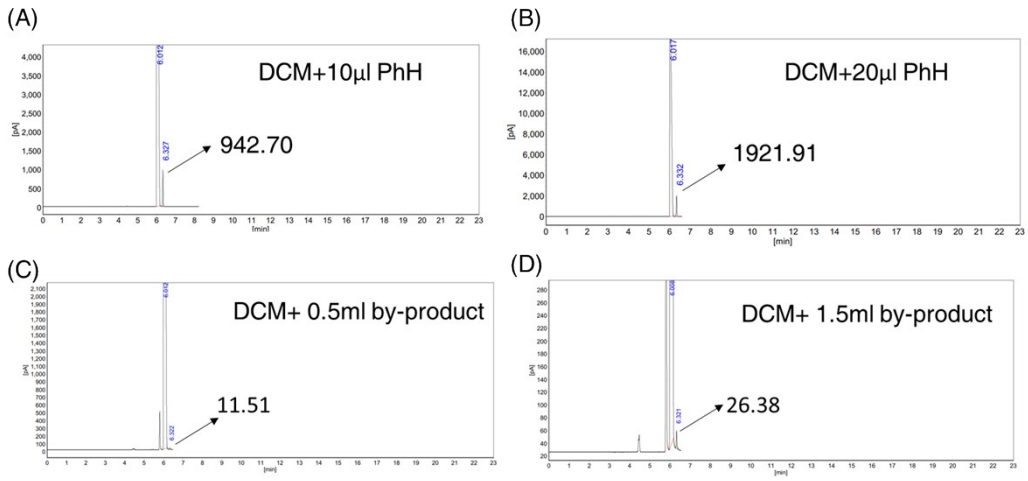

Figure S25. Detection of benzene in by-products of the nanocluster arylation from Au_{15}-SR to Au_{15}-Ph by gas chromatography (GC). (A,B). Determine the peak location of benzene in 6.3 pA. (C) A mixture of 3 mL of dichloromethane and 0.5 mL of by-product was used for the GC detection. (D) A mixture of 3 mL of dichloromethane and 1.5 mL of by-product was used for the GC detection. Compared with (C), the signal of benzene in 6.3 pA of (D) was triply higher, corresponding to the triple addition of the sample, confirming the presence of benzene in by-products of the nanocluster arylation from Au_{15}-SR to Au_{15}-Ph.

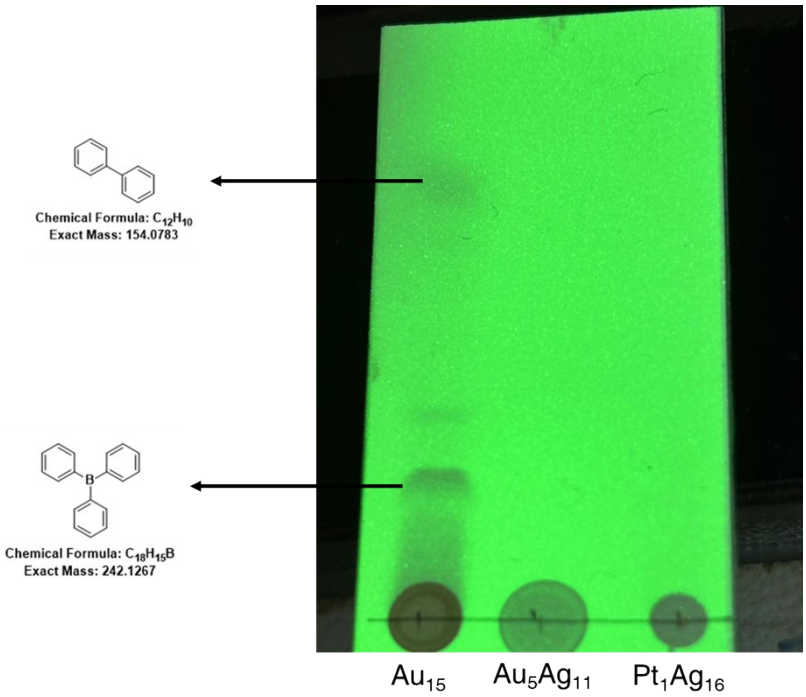

Figure S26. For the reported Au_5Ag_{11} and Pt_1Ag_{16} nanoclusters with similar thiol and DPPOE ligands of Au_{15}-SR, no C-B bond cleavage of the introduced $[BPh_4]^-$ was observed, demonstrating that the Au_5Ag_{11} and Pt_1Ag_{16} nanoclusters have no catalytic capacity towards the C-B bond cleavage of $[BPh_4]^-$.

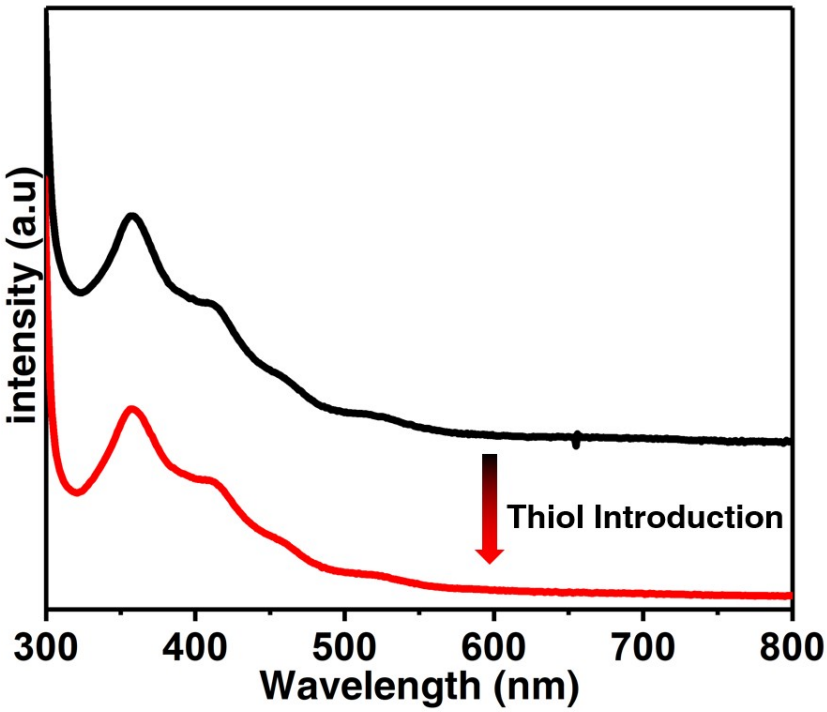

Figure S27. The maintained optical absorptions of Au_{15}-Ph by adding excess thiol ligands. In this context, the anti-arylation from Au_{15}-Ph to Au_{15}-SR was not practicable, demonstrating that the Au-aryl interactions in Au_{15}-Ph was much more robust than Au-S on the two ligand-exchanging sites of the cluster framework.

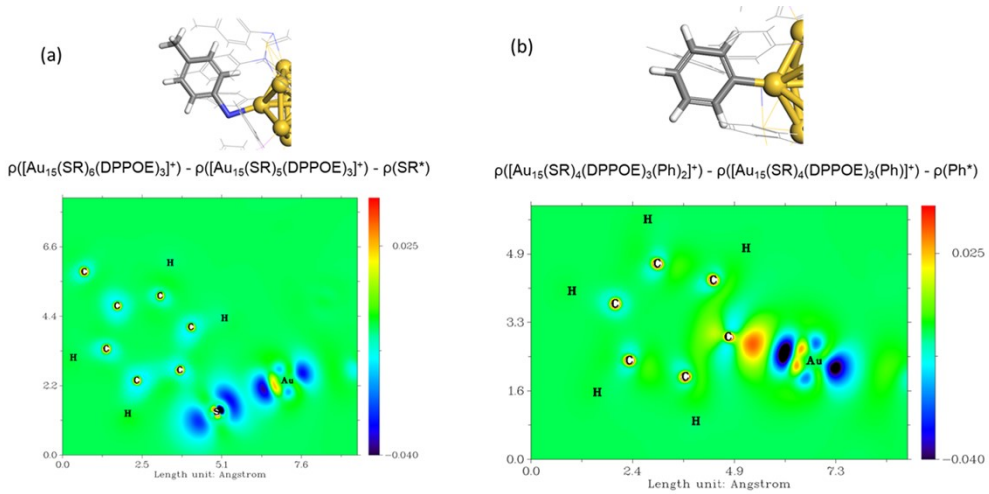

Figure S28. The charge density difference plots: (a) Au_{15}-SR; (b) Au_{15}-Ph clusters. Red color represents charge accumulation region and blue color represents charge depletion region.

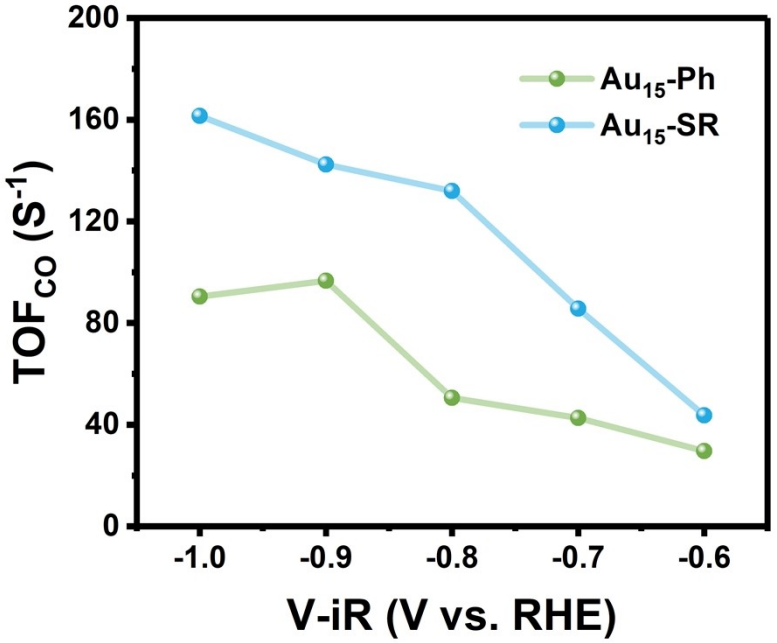

Figure S29. Turnover frequency (TOF) of Au_{15}-SR and Au_{15}-Ph nanoclusters in CO_2RR.

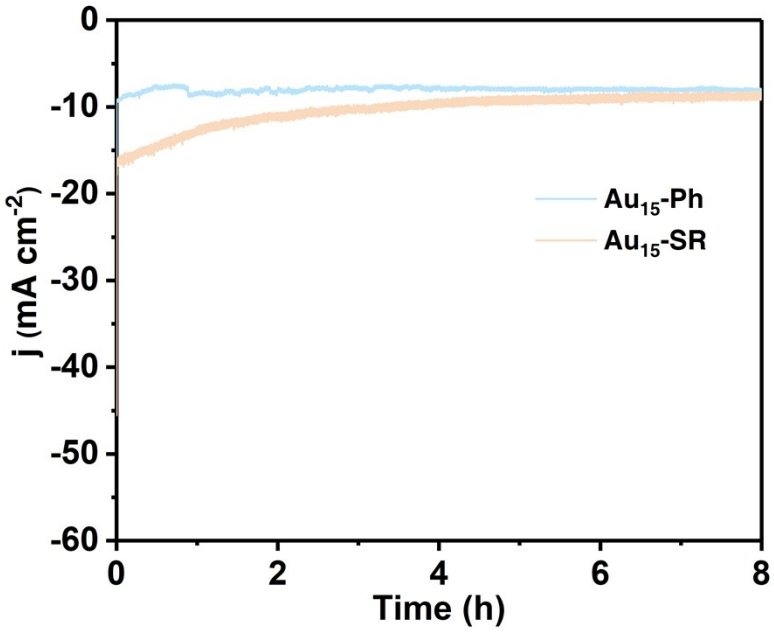

Figure S30. Stability test of Au_{15}-SR and Au_{15}-Ph nanoclusters in CO_2RR.

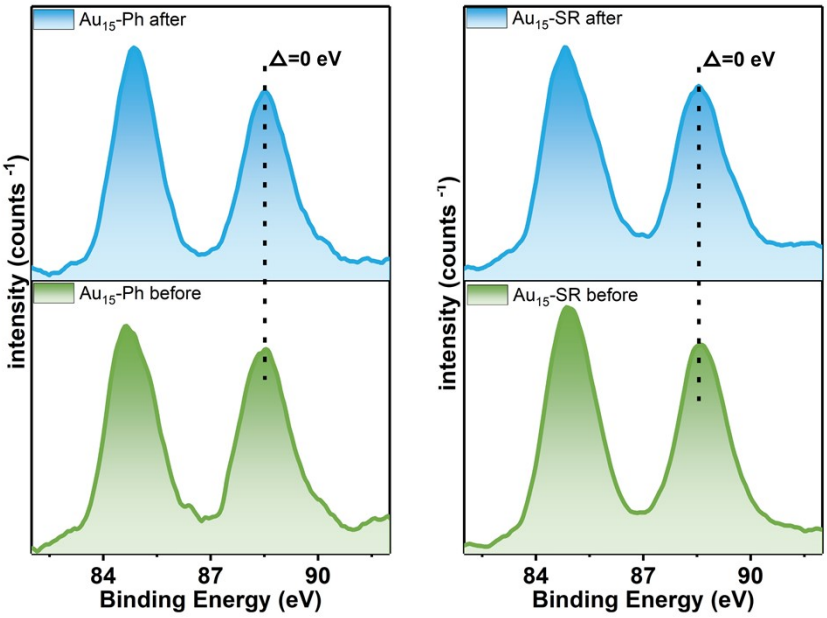

Figure S31. The maintained XPS spectra of Au 4f band for Au_{15}-SR and Au_{15}-Ph nanoclusters before and after catalysis demonstrated the stability of such cluster-based catalysts. We also compared the shapes and broadening of other cluster samples. The XPS results of Au_{15}-SR and Au_{15}-Ph nanoclusters were similar to those of other gold nanoclusters (see Table S6).

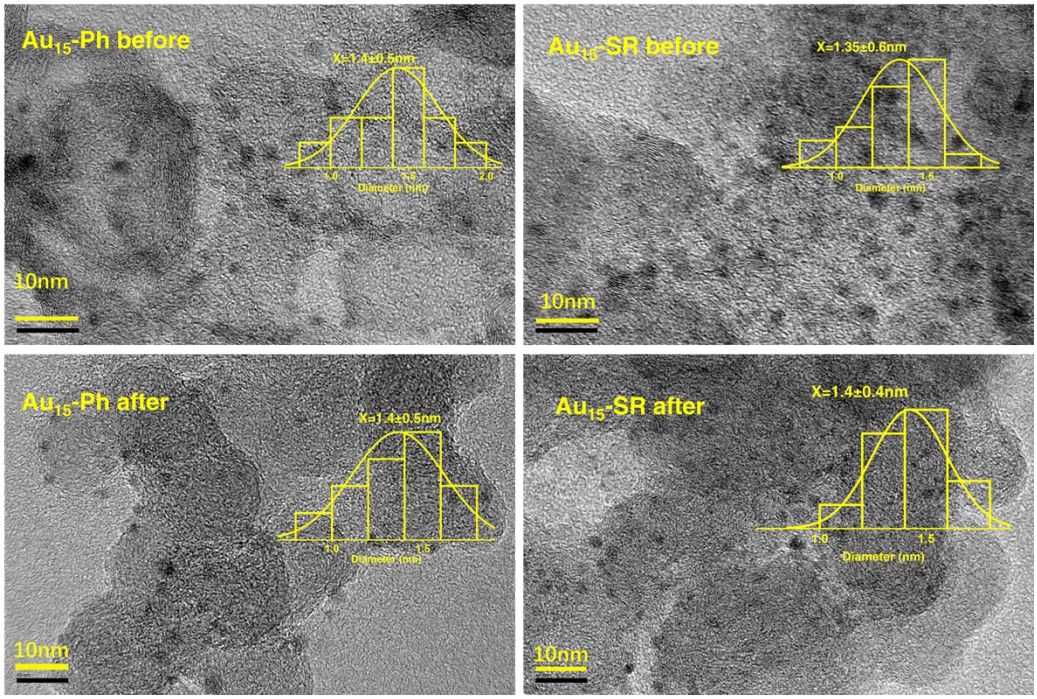

Figure S32. The maintained TEM and particle size analysis results Au_{15}-SR and Au_{15}-Ph nanoclusters before and after catalysis demonstrated the stability of such cluster-based catalysts.

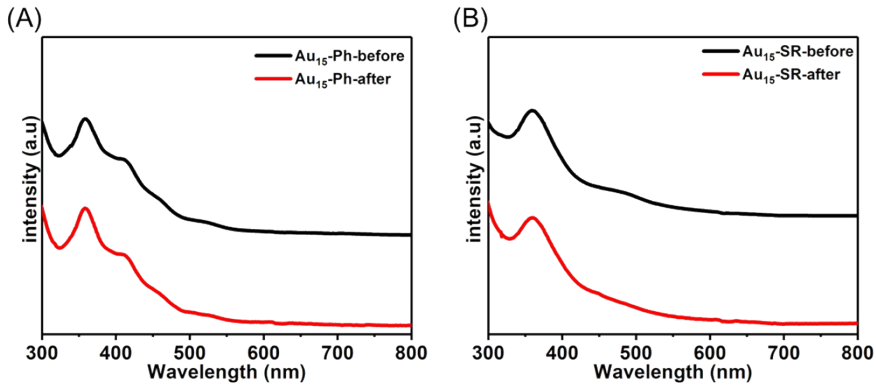

Figure S33. Optical absorptions of Au_{15}-Ph and Au_{15}-SR before and after the catalysis. The maintained spectra demonstrated the high robustness of the cluster-based catalysts.

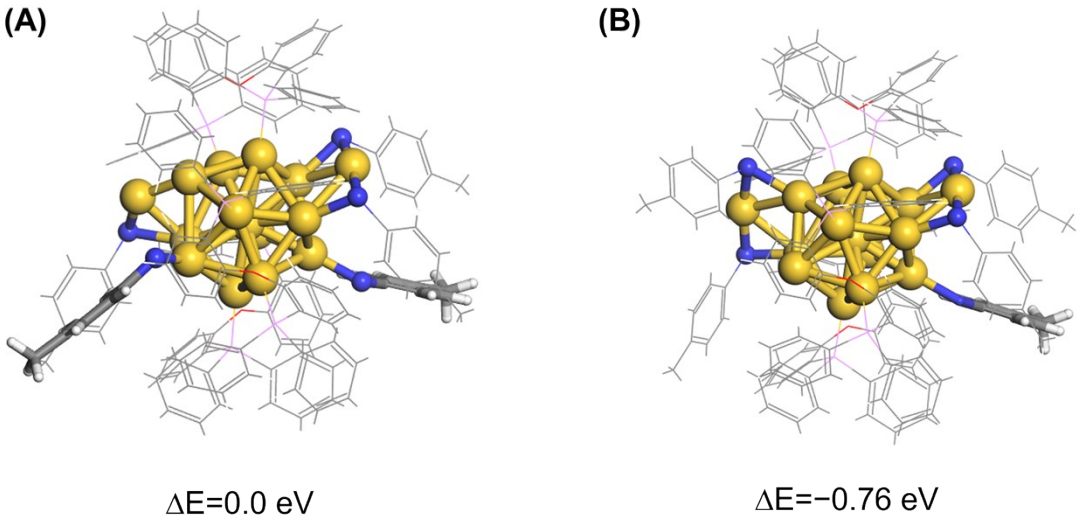

Figure S34. Optimized structures after dethiolating the -SR ligand from (A) staple motif and (B) independently anchored ligands in Au_{15}-SR nanocluster.

Table S1. Crystal data and structure refinement for the $Au_{15}(DPPOE)_3(SPh\text{-}^{p}Me)_4(Ph)_2$ nanocluster (Au_{15}-Ph).

Molecular formula	$C_{172}H_{142}Au_{15}BO_3P_6S_4$
Crystal system	triclinic
Space group	P-1
a/Å	16.8358(8)
b/Å	21.2426(11)
c/Å	24.1864(11)
α/°	84.400(4)
β/°	77.881(4)
γ/°	89.447(4)
Volume/Å^3	8416.3(7)
Z	2
ρ_{calc}g/cm^3	2.185
μ/mm-1	25.265
F(000)	5084.0
Radiation	CuK\a (λ = 1.54186)
Index ranges	-19 ≤ h ≤ 14, -19 ≤ k ≤ 24, -27 ≤ l ≤ 26
2θ range (°)	8.268 to 125
Measured reflections and unique reflections	26129 [Rint = 0.0769, Rsigma = 0.1014]
Goodness-of-fiton F^2	0.940
Largest diff. peak/hole / e Å^{-3}	4.71/-5.72
Final R indexes [I>=2σ (I)]	R1 = 0.0729, wR2 = 0.1778
Final R indexes [all data]	R1 = 0.1051, wR2 = 0.1993

Table S2. Crystal data and structure refinement for the $Au_{15}(DPPOE)_3(SPh\text{-}^{p}Me)_4(Ph\text{-}F)_2$ nanocluster (Au_{15}-Ph-F).

Molecular formula	$C_{172}H_{136}Au_{15}BF_6O_3P_6S_4$
Crystal system	triclinic
Space group	P-1
a/Å	16.7395(14)
b/Å	22.413(2)
c/Å	23.670(2)
α/°	99.314(7)
β/°	101.816(7)
γ/°	97.815(7)
Volume/Å^3	8445.0(13)
Z	2
ρ_{calc}g/cm^3	2.220
μ/mm-1	25.249
F(000)	5180.0
Radiation	CuK\a (λ = 1.54186)
Index ranges	-19 ≤ h ≤ 11, -24 ≤ k ≤ 25, -21 ≤ l ≤ 27
2θ range (°)	8.416 to 124.996
Measured reflections and unique reflections	25743 [R_{int} = 0.0890, R_{sigma} = 0.0986]
Goodness-of-fiton F^2	0.941
Largest diff. peak/hole / e Å^{-3}	4.86/-2.68
Final R indexes [I>=2σ (I)]	R1 = 0.0746, wR2 = 0.1878
Final R indexes [all data]	R1 = 0.1101, wR2 = 0.2040

Table S3. Crystal data and structure refinement for the $Au_{15}(DPPOE)_3(SPh\text{-}^{p}Me)_4(Ph\text{-}Cl)_2$ nanocluster (Au_{15}-Ph-Cl).

Molecular formula	$C_{148}H_{120}Au_{15}Cl_2O_3P_6S_4$
Crystal system	triclinic
Space group	P-1
a/Å	20.4720(11)
b/Å	21.4293(13)
c/Å	22.5130(12)
α/°	115.818(4)
β/°	93.462(4)
γ/°	90.360(5)
Volume/Å^3	8868.6(9)
Z	2
ρ_{calc}g/cm^3	1.979
μ/mm-1	24.208
F(000)	4810.0
Radiation	CuK\a (λ = 1.54186)
Index ranges	-22 ≤ h ≤ 23, -24 ≤ k ≤ 19, -13 ≤ l ≤ 25
2θ range (°)	11.88 to 124.996
Measured reflections and unique reflections	27410 [Rint = 0.0509, Rsigma = 0.0729]
Goodness-of-fiton F^2	0.933
Largest diff. peak/hole / e Å^{-3}	3.57/-2.55
Final R indexes [I>=2σ (I)]	R1 = 0.0632, wR2 = 0.1701
Final R indexes [all data]	R1 = 0.0872, wR2 = 0.1821

Table S4. Comparison of the bond lengths of Au_{13} (from reference 7) and the Au_{13} kernel in Au_{15}-Ph.

	Length Å	Average Å
Au_{15}-Ph	2.753-3.12	2.878
Au_{13}	2.696-2.974	2.865

Table S5. FECO Comparison of various gold nanoclusters in catalyzing the reduction of CO_2 to CO.

Catalysts	FECO (@V vs RHE)	ref
$Au_{28}(C_2B_{10}H_{11}S)_{12}(tht)_4Cl_4$	98.5%@-0.9	8
$[Au_{11}(dppe)_5]^{3+}$	70%@-0.60	9
$Au_{52}(CHT)_{28}$	94.2%@-0.67	10
$Au_{78}(TBBT)_{40}$	95%@-0.57	11
$Au_{25}(Nap)_{18}$	95%@-0.8	12
$Au_{44}(PPh_3)(TBBT)_{26}$	97%@-0.57	13
Au_{15}-SR	96%@-0.7V	This work
Au_{15}-Ph	93%@-0.7V	This work

Table S6. Comparison of the Au peak positions of different clusters.

	Au $4f_{7/2}$	reference
Au_{11}	84.2	14
Au_{13}	85.5	14
$Au_{13}Cu_1$	84.9	14
$Au_{13}Cu_2$	84.5	14
$Au_{13}Cu_3$	85.0	14
$Au_{13}Cu_4$	84.9	14
Au NPs-1	83.6	15
Au_{44}	84.59	16
Au_{52}	84.67	16
Au_{78}	84.71	16
Au_{92}	84.76	16
Au NPs-2	84.9	16
Au_3	84.85	17
Au_8Ag_{55}	85.44	18
Au_8Ag_{57}	85.7	18
$Au_{12}Ag_{60}$	85.9	18
Au^0	84.0	19
Au^1	86.0	19
Au_{15}-SR	84.8	
Au_{15}-Ph	84.7	

DFT optimized geometry

Au_{15}-Ph

298

opt.log Energy: -7281597.1951265

Au	0.00183	0.02454	-0.00228
Au	-2.07097	-1.51198	1.26374
Au	2.56832	-0.13098	1.13480
Au	0.74925	-2.39375	1.20557
Au	0.14231	0.09277	2.81185
Au	-2.57150	0.07490	-1.13645
Au	-2.04377	1.48810	1.42467
Au	0.89831	2.35764	1.23383
Au	-0.91036	-2.30489	-1.26864
Au	1.96342	-1.62135	-1.30584
Au	-0.13587	0.17120	-2.81363
Au	-1.79337	-1.77233	4.26372
Au	2.14701	1.37615	-1.39424
Au	-0.72304	2.44408	-1.17944
Au	1.66763	-1.78424	-4.31476
P	1.39342	-4.37878	2.23009
S	-0.15883	-0.35100	5.23974
P	4.62558	-0.20722	2.23025
S	-3.25340	-3.04557	2.89945
S	3.03493	-3.18932	-2.98561
P	1.62607	4.37910	2.14746
P	-1.70478	-4.21719	-2.32515
P	-4.62878	0.18560	-2.22937
P	-1.29465	4.53850	-2.03738
O	3.83372	2.53943	2.82361
O	-0.21279	-5.31276	-0.04536
C	-3.71905	2.76935	3.60060
H	-2.83396	2.62962	4.22629
C	-4.86900	3.34792	4.16584
H	-4.85539	3.65307	5.21749
C	-6.02909	3.52345	3.39460
H	-6.92320	3.97519	3.83568
C	-6.03184	3.10371	2.05532
H	-6.92525	3.22970	1.43524
C	-4.88042	2.52683	1.49279
H	-4.90003	2.22401	0.44348
C	-3.70316	2.35814	2.25174
C	0.04156	-5.61508	2.31992
C	-0.57848	-5.99576	1.10807

C	-1.58600	-6.96631	1.08144
H	-2.05495	-7.22619	0.12984
C	-2.00138	-7.55674	2.28096
H	-2.80061	-8.30278	2.26157
C	-1.40887	-7.18520	3.49647
H	-1.73323	-7.64627	4.43296
C	-0.39007	-6.22373	3.51330
H	0.08397	-5.94727	4.45832
C	2.71788	-5.30087	1.36313
C	3.40056	-4.70796	0.29007
H	3.14924	-3.68647	-0.01461
C	4.37720	-5.43605	-0.40463
H	4.88969	-4.97042	-1.24999
C	4.68526	-6.74625	-0.01672
H	5.44663	-7.31365	-0.56035
C	4.01716	-7.33613	1.06997
H	4.25923	-8.35822	1.37597
C	3.02902	-6.62014	1.75684
H	2.49172	-7.08294	2.59084
C	-0.40783	2.33660	5.81203
H	0.58195	2.43171	5.35590
C	-1.04653	3.45742	6.35202
H	-0.54049	4.42715	6.31093
C	-2.32830	3.36714	6.93136
C	-2.95183	2.10654	6.95490
H	-3.95263	2.00864	7.38800
C	-2.32860	0.97282	6.41593
H	-2.83721	0.00405	6.42288
C	-1.05087	1.08355	5.84135
C	2.01572	-4.15725	3.93626
C	3.37273	-4.37036	4.24984
H	4.06381	-4.71868	3.47816
C	3.83594	-4.12917	5.55098
H	4.89168	-4.29287	5.78694
C	2.95495	-3.68405	6.54602
H	3.32199	-3.49907	7.55929
C	1.60646	-3.45417	6.23263
H	0.91337	-3.08043	6.99185
C	1.14106	-3.67647	4.93198
H	0.09256	-3.46237	4.68833
C	-5.74955	-1.12414	-1.62752
C	-6.33620	-2.07562	-2.48228
H	-6.13151	-2.04532	-3.55580
C	-7.18060	-3.06093	-1.95006

H	-7.62932	-3.80533	-2.61439
C	-7.45610	-3.08647	-0.57601
H	-8.12381	-3.85040	-0.16718
C	-6.86332	-2.14472	0.28056
H	-7.06206	-2.16561	1.35505
C	-5.99329	-1.17944	-0.23853
H	-5.50367	-0.46910	0.43606
C	-3.77460	-4.38281	-0.42797
H	-3.45625	-3.38067	-0.12106
C	-3.11499	-5.03045	-1.48406
C	-3.51707	-6.32383	-1.88142
H	-2.99903	-6.82902	-2.70286
C	-4.57029	-6.96106	-1.21392
H	-4.88249	-7.96296	-1.52316
C	-5.21308	-6.31920	-0.14164
H	-6.02505	-6.82606	0.38842
C	-4.81575	-5.03413	0.24919
H	-5.30855	-4.52885	1.08317
C	2.38629	4.17474	3.80841
C	3.47324	3.28370	3.93893
C	4.11544	3.08982	5.16792
H	4.93603	2.37116	5.23728
C	3.67167	3.79980	6.29058
H	4.16222	3.63967	7.25454
C	2.60022	4.69914	6.18273
H	2.25763	5.25548	7.05922
C	1.96444	4.88565	4.94793
H	1.13222	5.58894	4.85728
C	5.63082	-1.59954	1.60948
C	5.86613	-1.65943	0.21927
H	5.44312	-0.89862	-0.44500
C	6.63939	-2.69618	-0.31516
H	6.83093	-2.72325	-1.39087
C	7.14196	-3.70107	0.52709
H	7.73199	-4.52037	0.10627
C	6.87470	-3.66616	1.90258
H	7.25312	-4.45777	2.55609
C	6.12816	-2.61257	2.45008
H	5.92842	-2.57810	3.52428
C	-4.61306	0.08364	-4.05805
C	-5.79562	0.33009	-4.78859
H	-6.73473	0.52445	-4.26109
C	-5.75890	0.34627	-6.18871
H	-6.67673	0.53397	-6.75377

C	-4.54278	0.14117	-6.86192
H	-4.51294	0.17406	-7.95517
C	-3.36943	-0.10108	-6.13561
H	-2.41582	-0.25850	-6.64537
C	-3.40459	-0.14158	-4.73440
H	-2.48948	-0.32088	-4.16137
C	-0.46757	-5.56843	-2.41437
C	-0.08212	-6.20343	-3.60980
H	-0.51694	-5.87355	-4.55657
C	0.83955	-7.25847	-3.59287
H	1.12929	-7.73904	-4.53090
C	1.37845	-7.69802	-2.37513
H	2.10165	-8.51797	-2.35524
C	1.00791	-7.08231	-1.17364
H	1.43829	-7.39657	-0.22022
C	0.09958	-6.01823	-1.20025
C	-5.88864	-3.09715	3.71641
H	-5.72928	-4.17458	3.82219
C	-4.83333	-2.27361	3.28549
C	-5.04379	-0.88807	3.15753
H	-4.23053	-0.24002	2.81578
C	-6.29275	-0.33858	3.46191
H	-6.43264	0.74154	3.35100
C	-7.36273	-1.14844	3.89746
C	-7.13863	-2.53289	4.01516
H	-7.95404	-3.18380	4.34862
C	6.99463	1.23441	1.49374
H	7.41288	0.27640	1.17383
C	7.75805	2.40584	1.39705
H	8.77641	2.35812	1.00203
C	7.21583	3.63213	1.81044
H	7.80169	4.55132	1.72416
C	5.91389	3.69637	2.32162
H	5.46931	4.64860	2.62031
C	5.15831	2.52169	2.41273
C	5.68441	1.27609	2.00536
C	-3.64846	-4.03589	-4.37196
H	-4.37548	-4.33703	-3.61337
C	-4.07234	-3.75204	-5.67783
H	-5.13370	-3.83356	-5.93041
C	-3.14508	-3.36795	-6.65617
H	-3.48148	-3.14963	-7.67350
C	-1.78803	-3.24241	-6.32122
H	-1.05735	-2.91723	-7.06751

C	-1.36022	-3.50895	-5.01583
H	-0.30190	-3.37804	-4.75608
C	-2.28397	-3.92890	-4.03704
C	-8.69736	-0.53751	4.24744
H	-8.94583	0.29651	3.57161
H	-8.68922	-0.12935	5.27372
H	-9.51054	-1.27819	4.19584
C	7.27774	-1.55907	-3.88860
C	6.26529	-0.69101	-3.42877
H	6.48078	0.37173	-3.27840
C	4.97690	-1.15935	-3.15497
H	4.20786	-0.46673	-2.79808
C	4.66752	-2.51942	-3.34054
C	5.66112	-3.39834	-3.80716
H	5.42136	-4.45365	-3.96931
C	6.95125	-2.91510	-4.07604
H	7.71663	-3.60740	-4.44300
C	-1.58216	5.15201	-4.82235
H	-0.70978	5.80064	-4.70535
C	-2.21485	5.03749	-6.06741
H	-1.83066	5.59632	-6.92487
C	-3.33515	4.20508	-6.21088
H	-3.82272	4.09975	-7.18385
C	-3.83276	3.49327	-5.11223
H	-4.69366	2.82662	-5.20818
C	-3.19503	3.61779	-3.87195
C	-2.05735	4.43637	-3.70680
C	0.22602	5.51838	2.43223
C	0.20879	6.84088	1.95166
H	1.05163	7.22138	1.36862
C	-0.89472	7.66432	2.22007
H	-0.90934	8.68992	1.83958
C	-1.97014	7.17981	2.97715
H	-2.82642	7.82722	3.18604
C	-1.96250	5.85488	3.44123
H	-2.81487	5.45204	3.99553
C	-0.87995	5.01776	3.15218
H	-0.89361	3.97390	3.48090
C	6.22770	2.75335	-2.00718
H	7.12623	2.82224	-1.38559
C	5.04260	2.24489	-1.44811
H	5.04255	1.93718	-0.39998
C	3.85893	2.14995	-2.20995
C	3.90223	2.56356	-3.55761

H	3.01157	2.47892	-4.18521
C	5.08601	3.07323	-4.11914
H	5.09307	3.38068	-5.17011
C	6.25290	3.17643	-3.34512
H	7.17369	3.57438	-3.78320
C	5.80681	-0.21229	4.78763
H	6.75990	-0.10709	4.25983
C	5.77401	-0.20943	6.18796
H	6.70695	-0.12189	6.75266
C	4.54455	-0.29969	6.86234
H	4.52025	-0.27812	7.95601
C	3.35160	-0.41289	6.13644
H	2.38766	-0.48107	6.64691
C	3.38052	-0.43858	4.73485
H	2.45103	-0.51583	4.16237
C	4.60423	-0.32991	4.05767
C	3.36659	4.85537	0.00785
H	2.89518	3.98289	-0.45692
C	2.92337	5.31146	1.25881
C	3.54330	6.42437	1.86932
H	3.21099	6.76500	2.85517
C	4.59768	7.07570	1.21848
H	5.07645	7.93949	1.68933
C	5.05020	6.60656	-0.02686
H	5.88820	7.10468	-0.52386
C	4.43746	5.50052	-0.62864
H	4.79632	5.11718	-1.58647
C	8.67350	-1.04548	-4.14417
H	9.24974	-0.97638	-3.20411
H	8.65355	-0.03561	-4.58423
H	9.23227	-1.70715	-4.82407
C	2.39368	5.78487	-3.28988
H	3.21746	5.33440	-3.85087
C	2.49145	7.09724	-2.80094
H	3.39065	7.68804	-2.99686
C	1.45029	7.64041	-2.03582
H	1.53461	8.65527	-1.63609
C	0.29198	6.89008	-1.78419
H	-0.52434	7.31698	-1.19556
C	0.18452	5.58154	-2.29024
C	1.25509	5.01932	-3.01838
H	1.19748	3.98372	-3.36786
C	-3.00405	4.59327	7.49488
H	-3.01358	5.41700	6.76058

H	-2.47770	4.96774	8.38996
H	-4.04502	4.38378	7.78552
C	-2.52419	5.53144	-1.11948
C	-3.06317	6.70599	-1.68973
H	-2.70630	7.05683	-2.66337
C	-4.07034	7.40618	-1.01513
H	-4.48663	8.31755	-1.45466
C	-4.55673	6.92630	0.21324
H	-5.35851	7.46429	0.72811
C	-4.02440	5.75924	0.77520
H	-4.41014	5.36874	1.71968
C	-3.00073	5.06367	0.11496
H	-2.59278	4.14388	0.54761
O	-3.61760	2.87093	-2.78020
C	-5.56542	1.74652	-1.98572
C	-4.94061	2.95233	-2.37252
C	-5.60287	4.18119	-2.26956
H	-5.08374	5.09950	-2.55349
C	-6.90897	4.21288	-1.76639
H	-7.42132	5.17408	-1.67068
C	-7.54873	3.02749	-1.37393
H	-8.57068	3.05428	-0.98629
C	-6.87895	1.80128	-1.48328
H	-7.37401	0.87489	-1.18047
S	0.13204	-0.23309	-5.25133
C	3.32468	4.54888	-7.38814
H	2.76112	5.07643	-8.17648
H	4.29476	4.24892	-7.81319
H	3.51808	5.28352	-6.58690
C	2.55816	3.35981	-6.86281
C	1.29469	3.53030	-6.26170
H	0.86542	4.53416	-6.18450
C	0.57849	2.44579	-5.74548
H	-0.39541	2.60160	-5.27212
C	1.12246	1.14863	-5.82245
C	2.37953	0.95759	-6.42091
H	2.81068	-0.04700	-6.46662
C	3.08143	2.05630	-6.93529
H	4.06489	1.89508	-7.38871

Au_{15}-SR

306

opt.log Energy: -7830430.4756348

Au	-0.00002	0.00008	0.01158

Au	-2.14439	-1.06669	1.52984
Au	0.26270	2.80576	0.04254
Au	-0.62146	1.35737	2.39483
Au	-2.39445	1.52396	-0.09881
Au	-0.26262	-2.80568	0.04714
Au	-2.12434	-1.15709	-1.45167
Au	-0.76826	1.25221	-2.40228
Au	0.62087	-1.35349	2.39723
Au	2.14412	1.06926	1.52830
Au	2.39451	-1.52410	-0.09585
Au	-4.56736	0.82015	1.83885
Au	2.12462	1.15463	-1.45331
Au	0.76854	-1.25637	-2.39993
Au	4.56717	-0.81674	1.84086
P	-1.08971	2.53075	4.35691
S	-4.43407	2.80942	0.53990
P	0.59242	5.11100	-0.05553
S	-4.14379	-1.18736	3.02583
S	4.14340	1.19294	3.02419
P	-1.41638	2.30538	-4.38407
P	1.08892	-2.52339	4.36143
P	-0.59242	-5.11106	-0.04715
P	1.41708	-2.31283	-4.37989
O	-0.19342	4.48654	-2.85927
O	-0.00048	0.00453	5.38069
C	-5.51792	-0.96104	-1.77875
H	-4.75100	-0.37206	-1.26189
C	-6.86300	-0.59574	-1.67047
H	-7.12286	0.28185	-1.07269
C	-7.88023	-1.32724	-2.30969
C	-9.33162	-0.94633	-2.14499
C	-7.49434	-2.44196	-3.08053
H	-8.26034	-3.02520	-3.60466
C	-6.15244	-2.82540	-3.18936
H	-5.87857	-3.69933	-3.78904
C	-5.13555	-2.09593	-2.52660
C	-1.85919	1.49435	5.65925
C	-1.15547	0.34141	6.07648
C	-1.64577	-0.47752	7.09951
H	-1.08412	-1.36868	7.38794
C	-2.86643	-0.16005	7.70718
H	-3.25724	-0.81032	8.49465
C	-3.58680	0.97267	7.30154
H	-4.53861	1.22190	7.77776

C	-3.08180	1.79687	6.28734
H	-3.63239	2.69150	5.98619
C	0.37704	3.21136	5.21853
C	1.63366	3.20229	4.59498
H	1.73447	2.80207	3.58087
C	2.75809	3.68170	5.28280
H	3.73542	3.65189	4.79508
C	2.62435	4.18945	6.58122
H	3.50272	4.56246	7.11638
C	1.36271	4.22177	7.19960
H	1.25558	4.62327	8.21163
C	0.23968	3.72762	6.52517
H	-0.74141	3.73277	7.01064
C	-5.28710	2.62075	-2.10821
H	-4.22614	2.54857	-2.36277
C	-6.26713	2.62145	-3.10615
H	-5.96225	2.52264	-4.15237
C	-7.63568	2.70993	-2.79188
C	-7.99614	2.82686	-1.43542
H	-9.05416	2.90897	-1.16441
C	-7.02827	2.82100	-0.42352
H	-7.32471	2.89379	0.62704
C	-5.66597	2.70446	-0.75883
C	-2.18152	3.97723	4.10581
C	-1.67317	5.28777	4.21374
H	-0.63416	5.44903	4.51109
C	-2.49856	6.38374	3.92880
H	-2.09588	7.39790	4.00941
C	-3.83209	6.18590	3.54389
H	-4.47131	7.04481	3.32180
C	-4.33674	4.88276	3.42405
H	-5.36655	4.71339	3.09744
C	-3.51383	3.78225	3.69064
H	-3.90617	2.76757	3.55370
C	-1.64419	-5.67300	1.33684
C	-1.18350	-6.57010	2.31853
H	-0.16988	-6.97431	2.25743
C	-2.03025	-6.94221	3.37291
H	-1.66846	-7.63607	4.13764
C	-3.33657	-6.43849	3.44142
H	-3.99602	-6.74109	4.25991
C	-3.79512	-5.53561	2.46884
H	-4.80943	-5.13028	2.51732
C	-2.94517	-5.13577	1.43145

H	-3.29453	-4.41332	0.68783
C	-1.63451	-3.19438	4.60025
H	-1.73517	-2.79591	3.58543
C	-0.37799	-3.20243	5.22400
C	-0.24085	-3.71641	6.53156
H	0.74017	-3.72074	7.01719
C	-1.36400	-4.20931	7.20670
H	-1.25704	-4.60904	8.21945
C	-2.62555	-4.17802	6.58808
H	-3.50401	-4.55006	7.12375
C	-2.75906	-3.67254	5.28874
H	-3.73632	-3.64355	4.80083
C	-2.14576	3.96572	-4.11429
C	-1.37261	4.93079	-3.43104
C	-1.82141	6.24923	-3.29245
H	-1.20117	6.97839	-2.76799
C	-3.08091	6.60105	-3.79355
H	-3.43925	7.62555	-3.66058
C	-3.88078	5.64988	-4.44268
H	-4.86716	5.92368	-4.82545
C	-3.40709	4.34217	-4.61095
H	-4.00983	3.60500	-5.14709
C	1.64388	5.67544	1.32769
C	2.94488	5.13845	1.42351
H	3.29445	4.41475	0.68122
C	3.79459	5.54017	2.46036
H	4.80891	5.13498	2.50973
C	3.33578	6.44471	3.43128
H	3.99505	6.74876	4.24938
C	2.02946	6.94823	3.36162
H	1.66746	7.64340	4.12505
C	1.18295	6.57424	2.30771
H	0.16931	6.97829	2.24569
C	0.91591	-6.14197	0.00687
C	0.84081	-7.53917	-0.17540
H	-0.13155	-8.02047	-0.32220
C	2.01501	-8.30231	-0.18276
H	1.95803	-9.38582	-0.32313
C	3.26274	-7.67541	-0.02320
H	4.17850	-8.27382	-0.04406
C	3.33550	-6.28836	0.16135
H	4.29960	-5.78885	0.28872
C	2.16258	-5.52145	0.18284
H	2.21284	-4.43723	0.31967

C	1.85824	-1.48472	5.66204
C	3.08079	-1.78613	6.29078
H	3.63144	-2.68126	5.99123
C	3.58566	-0.96016	7.30362
H	4.53741	-1.20855	7.78038
C	2.86520	0.17322	7.70723
H	3.25590	0.82485	8.49363
C	1.64460	0.48962	7.09887
H	1.08289	1.38125	7.38572
C	1.15444	-0.33108	6.07719
C	-6.34196	-2.84879	3.10104
H	-6.40860	-2.54482	4.15012
C	-5.32087	-2.32966	2.28495
C	-5.24578	-2.71498	0.93589
H	-4.45205	-2.31485	0.29717
C	-6.18982	-3.59993	0.40911
H	-6.12972	-3.86227	-0.65172
C	-7.22436	-4.12711	1.20738
C	-7.28038	-3.74044	2.55961
H	-8.07811	-4.13250	3.19945
C	2.63461	6.45016	-1.55038
H	3.07551	6.72792	-0.59000
C	3.24694	6.85313	-2.74346
H	4.16293	7.44874	-2.70580
C	2.68939	6.49151	-3.97852
H	3.17261	6.79360	-4.91173
C	1.51893	5.72577	-4.02534
H	1.08376	5.40327	-4.97465
C	0.91502	5.32838	-2.82793
C	1.45609	5.67997	-1.57369
C	1.67240	-5.28064	4.22300
H	0.63335	-5.44141	4.52043
C	2.49785	-6.37708	3.94001
H	2.09517	-7.39110	4.02224
C	3.83145	-6.17986	3.55501
H	4.47072	-7.03913	3.33446
C	4.33610	-4.87693	3.43309
H	5.36597	-4.70808	3.10637
C	3.51313	-3.77598	3.69769
H	3.90547	-2.76152	3.55913
C	2.18075	-3.97028	4.11297
C	-8.23532	-5.07734	0.61443
H	-7.79474	-6.07543	0.44339
H	-8.59122	-4.71134	-0.36281

H	-9.10734	-5.20749	1.27349
C	7.22403	4.12969	1.20103
C	6.18959	3.60113	0.40355
H	6.12958	3.86170	-0.65772
C	5.24554	2.71701	0.93171
H	4.45189	2.31578	0.29357
C	5.32052	2.33396	2.28142
C	6.34153	2.85448	3.09673
H	6.40809	2.55226	4.14632
C	7.27996	3.74525	2.55391
H	8.07762	4.13841	3.19316
C	3.40793	-4.34991	-4.60299
H	4.01075	-3.61362	-5.14025
C	3.88164	-5.65731	-4.43241
H	4.86812	-5.93173	-4.81450
C	3.08168	-6.60742	-3.78183
H	3.44005	-7.63167	-3.64704
C	1.82205	-6.25482	-3.28159
H	1.20175	-6.98313	-2.75603
C	1.37322	-4.93664	-3.42252
C	2.14649	-3.97268	-4.10722
C	-2.73892	1.41008	-5.28630
C	-2.89446	1.51983	-6.68318
H	-2.15182	2.06066	-7.27580
C	-4.00290	0.93680	-7.31114
H	-4.11775	1.02465	-8.39542
C	-4.96316	0.24881	-6.55213
H	-5.83382	-0.19513	-7.04389
C	-4.79695	0.10974	-5.16598
H	-5.52243	-0.44704	-4.56737
C	-3.67956	0.67697	-4.53474
H	-3.53799	0.53986	-3.45756
C	7.49497	2.43620	-3.08369
H	8.26106	3.01845	-3.60880
C	6.15312	2.81959	-3.19325
H	5.87937	3.69251	-3.79445
C	5.13612	2.09138	-2.52929
C	5.51832	0.95778	-1.77940
H	4.75132	0.36978	-1.26154
C	6.86336	0.59252	-1.67045
H	7.12310	-0.28404	-1.07109
C	7.88070	1.32277	-2.31091
C	9.33203	0.94193	-2.14556
C	-0.84093	7.53880	-0.18849

H	0.13141	8.01990	-0.33606
C	-2.01519	8.30184	-0.19739
H	-1.95829	9.38509	-0.33974
C	-3.26289	7.67513	-0.03682
H	-4.17869	8.27343	-0.05894
C	-3.33556	6.28842	0.15031
H	-4.29964	5.78907	0.27847
C	-2.16259	5.52164	0.17337
H	-2.21276	4.43767	0.31225
C	-0.91595	6.14194	-0.00364
C	1.15003	1.95620	-5.42501
H	1.27969	1.23553	-4.61113
C	-0.06493	2.64904	-5.56451
C	-0.20935	3.62739	-6.57209
H	-1.14143	4.19564	-6.65349
C	0.85259	3.88679	-7.44782
H	0.73937	4.64330	-8.23001
C	2.06186	3.18510	-7.31098
H	2.89410	3.39660	-7.98888
C	2.21163	2.22779	-6.29884
H	3.15805	1.70035	-6.16642
C	8.23497	5.07901	0.60660
H	7.79442	6.07687	0.43416
H	8.59077	4.71157	-0.37014
H	9.10706	5.21009	1.26539
C	4.79797	-0.11882	-5.16494
H	5.52353	0.43872	-4.56714
C	4.96420	-0.25997	-6.55087
H	5.83496	0.18308	-7.04326
C	4.00386	-0.94892	-7.30890
H	4.11872	-1.03839	-8.39305
C	2.89531	-1.53086	-6.68010
H	2.15260	-2.07246	-7.27193
C	2.73974	-1.41899	-5.28340
C	3.68046	-0.68490	-4.53290
H	3.53883	-0.54614	-3.45594
C	-8.68189	2.62548	-3.87467
H	-8.89697	1.57027	-4.12161
H	-8.34539	3.11408	-4.80293
H	-9.62998	3.09091	-3.56343
C	0.06590	-2.65847	-5.56002
C	0.21053	-3.63854	-6.56589
H	1.14261	-4.20696	-6.64608
C	-0.85120	-3.89938	-7.44146

H	-0.73783	-4.65724	-8.22232
C	-2.06045	-3.19737	-7.30615
H	-2.89252	-3.40997	-7.98391
C	-2.21043	-2.23831	-6.29569
H	-3.15685	-1.71057	-6.16447
C	-1.14905	-1.96529	-5.42204
H	-1.27888	-1.24323	-4.60943
O	0.19388	-4.49146	-2.85180
C	-1.45578	-5.68275	-1.56444
C	-0.91452	-5.33331	-2.81920
C	-1.51821	-5.73279	-4.01603
H	-1.08290	-5.41186	-4.96581
C	-2.68863	-6.49851	-3.96808
H	-3.17167	-6.80224	-4.90085
C	-3.24636	-6.85803	-2.73249
H	-4.16230	-7.45366	-2.69395
C	-2.63428	-6.45296	-1.54001
H	-3.07532	-6.72907	-0.57922
S	4.43400	-2.80840	0.54561
C	8.68278	-2.63313	-3.86841
H	8.89878	-1.57841	-4.11664
H	8.34605	-3.12263	-4.79611
H	9.63044	-3.09893	-3.55641
C	7.63631	-2.71538	-2.78570
C	6.26783	-2.62743	-3.10043
H	5.96316	-2.53062	-4.14690
C	5.28759	-2.62481	-2.10270
H	4.22669	-2.55310	-2.35764
C	5.66615	-2.70596	-0.75309
C	7.02838	-2.82189	-0.41726
H	7.32460	-2.89270	0.63349
C	7.99648	-2.82971	-1.42893
H	9.05443	-2.91135	-1.15754
S	-3.46844	-2.67689	-2.67021
S	3.46907	2.67229	-2.67406
H	-9.43912	0.13026	-1.93596
H	-9.79555	-1.48765	-1.30055
H	-9.92196	-1.18485	-3.04491
H	9.43928	-0.13416	-1.93382
H	9.79630	1.48529	-1.30263
H	9.92223	1.17798	-3.04622

References

1. Frisch, M. J.; Trucks, G. W.; Schlegel, H. B.; Scuseria, G. E.; Robb, M. A.; Cheeseman, J. R.; Scalmani, G.; Barone, V.; Petersson, G. A.; Nakatsuji, H.; Li, X.; Caricato, M.; Marenich, A. V.; Bloino, J.; Janesko, B. G.; Gomperts, R.; Mennucci, B.; Hratchian, H. P.; Ortiz, J. V.; Izmaylov, A. F.; Sonnenberg, J. L.; Williams; Ding, F.; Lipparini, F.; Egidi, F.; Goings, J.; Peng, B.; Petrone, A.; Henderson, T.; Ranasinghe, D.; Zakrzewski, V. G.; Gao, J.; Rega, N.; Zheng, G.; Liang, W.; Hada, M.; Ehara, M.; Toyota, K.; Fukuda, R.; Hasegawa, J.; Ishida, M.; Nakajima, T.; Honda, Y.; Kitao, O.; Nakai, H.; Vreven, T.; Throssell, K.; Montgomery Jr., J. A.; Peralta, J. E.; Ogliaro, F.; Bearpark, M. J.; Heyd, J. J.; Brothers, E. N.; Kudin, K. N.; Staroverov, V. N.; Keith, T. A.; Kobayashi, R.; Normand, J.; Raghavachari, K.; Rendell, A. P.; Burant, J. C.; Iyengar, S. S.; Tomasi, J.; Cossi, M.; Millam, J. M.; Klene, M.; Adamo, C.; Cammi, R.; Ochterski, J. W.; Martin, R. L.; Morokuma, K.; Farkas, O.; Foresman, J. B.; Fox, D. J. *Gaussian 16 Rev. C.01*, Wallingford, CT, 2016.
2. Perdew, J. P.; Burke, K.; Ernzerhof, M., Generalized Gradient Approximation Made Simple. *Phys. Rev. Lett.* **1996,** *77*, 3865-3868.
3. Hariharan, P. C.; Pople, J. A., The influence of polarization functions on molecular orbital hydrogenation energies. *Theor. Chim. Acta* **1973,** *28*, 213-222.
4. Hay, P. J.; Wadt, W. R., Ab initio effective core potentials for molecular calculations. Potentials for the transition metal atoms Sc to Hg. *J. Chem. Phys.* **1985,** *82*, 270-283.
5. Grimme, S.; Ehrlich, S.; Goerigk, L., Effect of the damping function in dispersion corrected density functional theory. *J. Comput. Chem.* **2011,** *32*, 1456-1465.
6. Tomasi, J.; Mennucci, B.; Cammi, R., Quantum Mechanical Continuum Solvation Models. *Chem. Rev.* **2005,** *105*, 2999-3094.
7. Shichibu, Y. and Konishi, K, HCl-Induced Nuclearity Convergence in Diphosphine-Protected Ultrasmall Gold Clusters: A Novel Synthetic Route to "Magic-Number" Au_{13} Clusters. Small, 6: 1216-1220
8. Wang, J.; Xu, F.; Wang, Z.-Y.; Zang, S.-Q.; Mak, T. C. W. Ligand-Shell Engineering of a Au_{28} Nanocluster Boosts Electrocatalytic CO_2 Reduction. Angew. Chem. Int. Ed. 2022, 61, e202207492.
9. Gao, Z.-H.; Wei, K.; Wu, T.; Dong, J.; Jiang, D.-e.; Sun, S.; Wang, L.-S. A Heteroleptic Gold Hydride Nanocluster for Efficient and Selective Electrocatalytic Reduction of CO_2 to CO. J. Am. Chem. Soc. 2022, 144, 5258-5262.
10. Xu, Z.; Dong, H.; Gu, W.; He, Z.; Jin, F.; Wang, C.; You, Q.; Li, J.; Deng, H.; Liao, L.; Chen, D.; Yang, J.; Wu, Z. Lattice Compression Revealed at the ≈1 nm Scale. Angew. Chem. Int. Ed. 2023, 62, e202308441.
11. Wang, W.; Chen, D.; Fung, V.; Zhuang, S.; Zhou, Y.; Wang, C.; Bian, G.; Zhao, Y.; Xia, N.; Li, J.; Deng, H.; Liao, L.; Yang, J.; Jiang, D.-e.; Wu, Z. Gapped and Rotated Grain Boundary Revealed in Ultra-Small Au Nanoparticles for Enhancing Electrochemical CO_2 Reduction. Angew. Chem. Int. Ed. 2024, e202410109.
12. Li, S.; Nagarajan, A. V. ; Li, Y.; Kauffman, D. R.; Mpourmpakis, G.; Jin, R. The role of ligands in atomically precise nanocluster-catalyzed CO2 electrochemical reduction. Nanoscale 2021, 13, 2333-2337.
13. Zhuang, S.; Chen, D.; Ng, W.-P.; Liu, L.-J.; Sun, M.-Y.; Liu, D.; Nawaz, T.; Xia, Q.; Wu, X.; Huang, Y.-L.; Lee, S.; Yang, J.; Yang, J.; He, J. Phosphine-Triggered Structural Defects in Au44 Homologues Boost Electrocatalytic CO_2 Reduction. Angew. Chem. Int. Ed. 2023, 62, e202306696.
14. Tan, Y.; Sun, G.; Jiang, T.; Liu, D.; Li, Q.; Yang, S.; Chai, J.; Gao, S.; Yu, H.; Zhu, M. Symmetry

Breaking Enhancing the Activity of Electrocatalytic CO2 Reduction on an Icosahedron-Kernel Cluster by Cu Atoms Regulation. Angew. Chem. Int. Ed. 2024, 63, e202317471.
15. Shangguan, W.; Liu, Q.; Wang, Y. et al. Molecular-level insight into photocatalytic CO2 reduction with H2O over Au nanoparticles by interband transitions. Nat Commun 13, 3894 (2022).
16. Wang, W.; Chen, D.; Fung, V.; Zhuang, S.; Zhou, Y.; Wang, C.; Bian, G.; Zhao, Y.; Xia, N.; Li, J.; Deng, H.; Liao, L.; Yang, J.; Jiang, D.-e.; Wu, Z. Gapped and Rotated Grain Boundary Revealed in Ultra-Small Au Nanoparticles for Enhancing Electrochemical CO2 Reduction. Angew. Chem. Int. Ed. 2025, 64, e202410109.
17. Chen, R.; Ma, X.-H.; Luo, P.; Gong, C.-H.; Sun, J.-J.; Si, Y.-B.; Dong, X.-Y.; Pan, F.; Zang, S.-Q. Atomically Precise Ternary Cluster: Polyoxometalate Cluster Sandwiched by Gold Clusters Protected by N-Heterocyclic Carbenes. Angew. Chem. Int. Ed. 2024, 63, e202408310.
18. Hu, J.; Zhou, M.; Li, K.; Yao, A.; Wang, Y.; Zhu, Q.; Zhou, Y.; Huang, L.; Pei, Y.; Du, Y.; Jin, S.; Zhu, M. Evolution of Electrocatalytic CO2 Reduction Activity Induced by Charge Segregation in Atomically Precise AuAg Nanoclusters Based on Icosahedral M13 Unit 3D Assembly. Small 2023, 19, 2301357.
19. Casaletto, M.P.; Longo, A.; Martorana, A.; Prestianni, A. and Venezia, A.M. (2006), XPS study of supported gold catalysts: the role of Au0 and Au+δ species as active sites. Surf. Interface Anal., 38: 215-218.